GWM-HFN: A Novel Gray-White Matter Heterogeneous Fusion Network for Functional Connectomes

Ze-Qiang LinLi[1*], Zhuo-Yan Cai[1], Chu-Chu Zheng[3], Kang Hu[2,4*]

Author Affiliations:

[1] School of Mathematics and Statistics, Guangdong University of Foreign Studies, Guangzhou, P.R. China

[2] School of Information Engineering, Wuhan Business University, Wuhan, P.R. China

[3] School of Public Health, Shanxi Medical University, Taiyuan, P.R. China

[4] MOE-LCSM, School of Mathematics and Statistics, Hunan Normal University, Changsha, P. R. China

Corresponding author:

Ze-Qiang LinLi, Ph.D., School of Mathematics and Statistics, Guangdong University of Foreign Studies, Guangzhou 510004, P.R. China. Email: linlizeqiang@163.com Phone: +86-16620164042

Kang Hu, Ph.D., School of Information Engineering, Wuhan Business University, Wuhan, P.R. China, Wuhan 430056, P.R. China. Email: hk2016423@163.com

Abstract

Resting-state functional connectivity (FC) studies have predominantly centered on gray matter (GM), largely overlooking the functional contributions of white matter (WM). However, emerging evidence indicates WM blood-oxygen-level-dependent (BOLD) signals actively shape large-scale brain networks. Current methods to integrate WM face limitations, including challenges in assessing global network properties from bipartite GM-WM connections or the nascent stage of unified connectome models. Here, we introduce the Gray-White Matter Heterogeneous Fusion Network (GWM-HFN), a novel framework that models WM as a dynamic bridge, defining GM-GM functional links via the covariance of their interaction profiles with WM tracts. Validated across six independent datasets, GWM-HFN demonstrates fair short-term (ICC ~0.36) and slight-to-fair long-term (ICC ~0.20) test-retest reliability, comparable to conventional GM-based FC. GWM-HFN exhibits distinct topological features, including small-worldness and enhanced modular segregation compared to GM-GM networks, capturing over 40% unique variance and significantly increased sensitivity to inter-individual variability. Lifespan analyses reveal global linear declines and complex non-linear age effects in GWM-HFN connectivity, with peak connectivity in early adulthood (~34 years). Clinically, individuals with autism spectrum disorder (ASD) show GWM-HFN-specific hyperconnectivity, which correlates with symptom severity and offers greater sensitivity than GM-GM FC. Furthermore, GWM-HFN connectivity patterns predict individual differences in cognitive performance, notably in language tasks. The GWM-HFN framework provides a robust and more comprehensive approach to understanding WM-mediated neural communication, bridging structural and functional connectomics, and offers promising avenues for developing neuroimaging biomarkers for aging and neuropsychiatric disorders

Keywords: White Matter Functional Connectivity, Gray-White Matter Fusion, Functional Connectome, Brain Network, Resting-State fMRI

1. Introduction

Over the last twenty years, resting-state functional magnetic resonance imaging (rs-fMRI) has emerged as a pivotal tool for mapping synchronized neural activity across various brain regions, mapping synchronized neural activity, commonly termed functional connectivity (FC)[1,2]. This innovative imaging technique has significantly enriched our understanding of the brain's functional connectome, which provides a network-level perspective on the interconnections among brain regions. As a result, researchers have gained deeper insights into the large-scale organizational structure of the brain, the trajectories of development and aging, and the alterations associated with neuropsychiatric disorders[3–6].

Historically, the majority of studies focusing on the functional connectome have centered on gray matter (GM), where it is commonly assumed that neural activity drives blood-oxygen-level-dependent (BOLD) signals. This GM-centric focus has inadvertently led to a relative neglect of white matter (WM) in connectivity analyses, primarily due to its lower BOLD signal amplitude and its traditional classification as a mere structural conduit facilitating communication between GM regions[7–9]. However, a growing body of evidence is challenging this long-held perspective, suggesting that WM may play a more active role in the dynamics of functional networks than previously acknowledged[10–15].

Recent research, aiming to incorporate WM, has explored several avenues, including WM-only networks, GM-WM interactions, and more unified connectomes, each with its own set of advancements and unresolved challenges. The first approach investigates WM-only functional networks, treating WM parcels as independent nodes and analyzing their intrinsic functional interactions. These studies have demonstrated that WM possesses unique functional connectivity patterns, establishing stable networks that are comparable to those found in GM[12]. Moreover, alterations in WM functional connectivity have been identified in various neurological and psychiatric disorders, such as schizophrenia[16] and nicotine dependence[17]. However, analyzing WM in isolation may obscure its broader contributions to the coordination of large-scale brain communication. To address this limitation, researchers have introduced a GM-WM network approach, which explicitly models the functional interactions between GM and WM nodes, each defined by distinct atlases[13]. This paradigm has revealed significant functional disruptions

in psychiatric populations[18,19], while also providing new insights into how WM contributes to the dynamics of GM networks[20]. Nevertheless, these networks remain structurally constrained, as they primarily capture GM-to-WM connections and lack closed-loop interactions[21]. This structural limitation complicates the application of conventional network analyses, such as assessments of global efficiency or modularity. Additionally, differences in signal amplitude and dynamic properties between WM-WM and GM-GM connections can lead to inconsistencies[11] when analyzed within a unified framework, ultimately affecting the biological interpretation of network topology.

To overcome these challenges, a third approach—the unified functional connectome—has emerged, aiming to integrate both GM and WM connectivity into a cohesive framework that can capture closed-loop interactions and elucidate comprehensive mechanisms of network integration[22–24]. However, this area of research is still in its infancy, lacking a standardized modeling paradigm. Several promising methods have been put forth, each presenting unique advantages while grappling with methodological hurdles. For instance, Gao et al. introduced a projection-based mapping strategy that mathematically transforms GM-WM functional connections into an equivalent GM-only network, termed the "WM-mediated GM functional connectivity network." By calculating its global efficiency, they discovered a negative correlation between network efficiency and age[22] as well as a reduction in efficiency among individuals with preclinical Alzheimer's disease[25]. This innovative approach partially addresses the absence of triangular pathways in bipartite GM-WM networks and highlights distinct topological properties. However, as a directed network, it also presents interpretational challenges from both methodological and clinical standpoints. Another avenue of research has focused on the modulation of GM network organization by WM. Wang et al. developed an edge-centric network analysis approach that illustrates how WM signals significantly regulate GM functional organization, with evidence suggesting that this modulation is impaired in disease populations[24]. Although this method elucidates the modulatory role of WM in brain information transfer, it does not explicitly integrate GM and WM connectivity within a unified network framework. More recently, Zu et al. proposed a three-way correlation model that treats WM BOLD signals as a third component within traditional GM functional networks, thereby providing a more comprehensive representation of WM's mediation of GM interactions[23]. This approach offers a

richer depiction of the whole-brain functional architecture but has yet to undergo rigorous testing for test-retest reliability, topological properties, and robustness of application. As research in this area continues to evolve, the integration of GM and WM connectivity promises to enhance our understanding of the brain's complex functional dynamics, ultimately paving the way for improved insights into neuropsychiatric conditions and their underlying mechanisms.

Motivated by these foundational studies, we propose a novel functional connectome framework that integrates functional information from two heterogeneous structures, GM and WM, which we term the gray-white matter heterogeneous fusion network (GWM-HFN). By treating WM as a dynamic bridge rather than a passive relay, we aim to uncover subtle interactions that remain undetected in conventional GM-based network models. To validate our framework, our study rigorously examines the test-retest reliability and topological organization of the GWM-HFN. We juxtapose our findings against those derived from conventional GM-GM connectivity analyses, providing a comprehensive comparison that highlights the unique contributions of our model. Furthermore, we delve into the practical implications of GWM-HFN by investigating age-related changes in connectivity patterns, assessing its clinical relevance, and exploring its correlations with various cognitive and behavioral measures. Through these multifaceted analyses, we aspire to establish a robust and comprehensive framework that not only enhances our understanding of the brain’s functional architecture but also effectively bridges the existing divide between traditional GM-centric methodologies and the active, communicative role of white matter in inter-regional connectivity.

2. Results

2.1 General Description of Analytical Methods, Datasets and Research Questions

In this research, we presented GWM-HFN, a network framework aimed at merging functional data from two heterogeneous brain structures (GM and WM) by deliberately integrating WM signals into rs-fMRI connectivity evaluations. **Figure 1** illustrates a schematic representation of this method. In summary, following preprocessing, time-series signals were gathered from 90 GM regions (Anatomical Automatic Labeling, AAL atlas; refer to Table S1 for specifics) and 48 WM bundles (JHU-ICBM 48 atlas; refer to Table S2 for specifics). Subsequently, we developed a bipartite GM-WM correlation matrix, where each row represents the functional connectivity profile of a GM region with various WM bundles. Considering that WM acts as the main pathway for long-distance communication between GM regions, we also calculated the covariance of GM-WM connectivity profiles, converting the bipartite matrix into a GM-centered representation that indirectly reflects WM-mediated interactions. The resulting GWM-HFN encapsulates the functional communication strength among GM regions while maintaining information regarding their interconnected WM pathways. This modification retains WM-derived functional information within a GM-aligned network framework, allowing for the exploration of both global and local network characteristics while incorporating the impact of WM pathways on brain activity.

We meticulously assessed GWM-HFN through various independent datasets to evaluate its dependability, network characteristics, and functional significance, which encompassed test-retest reliability (TRT), structural organization, comparisons to GM-GM connectivity, age-related variations, clinical significance, and cognitive/behavioral associations. In particular, the Southwest University Longitudinal Imaging Multimodal (SLIM) dataset (http://dx.doi.org/10.15387/fcp_indi.retro.slim) was utilized to analyze network patterns, structural organization, and long-term reliability, while the Beijing Normal University (BNU-3) (http://dx.doi.org/10.15387/fcp_indi.corr.bnu3) offered measurements for short-term reliability. The Southwest University Adult Lifespan (SALD) dataset (https://fcon_1000.projects.nitrc.org/indi/retro/sald.html) was employed to examine age-related trajectories of GWM-HFN connectivity within a cross-sectional population. To investigate clinical

relevance, we focused on disorder-specific changes in GWM-HFN using the Autism Brain Imaging Data Exchange II (ABIDE-II) project (https://fcon_1000.projects.nitrc.org/indi/abide/abide_II.html), with an emphasis on autism spectrum disorder (ASD). Lastly, the Brain Genomics Superstruct Project (BGSP) dataset (https://www.neuroinfo.org/gsp/) facilitated partial least squares (PLS) regression to connect GWM-HFN connectivity with cognitive and behavioral metrics. A comprehensive description of these datasets is available in the Supporting Information (Study datasets Section), with Table S3 providing a summary of essential demographic details.

To facilitate cross-network comparisons and interpretability, GM nodes were organized into seven functional networks according to Yeo's functional parcellation of the cerebral cortex, which includes the Visual Network (VN), Sensorimotor Network (SMN), Attention Network (AN), Limbic Network (LN), Frontoparietal Network (FPN), Default Mode Network (DMN), and Basal Ganglia Network (BGN) (Figure 2A, Table S1). This categorization facilitated a more structured evaluation of GWM-HFN connectivity trends among functionally diverse systems. Additional information regarding node assignments and the relevant methods can be accessed in the Supporting Information (Mapping AAL Atlas to Macroscopic Networks section).

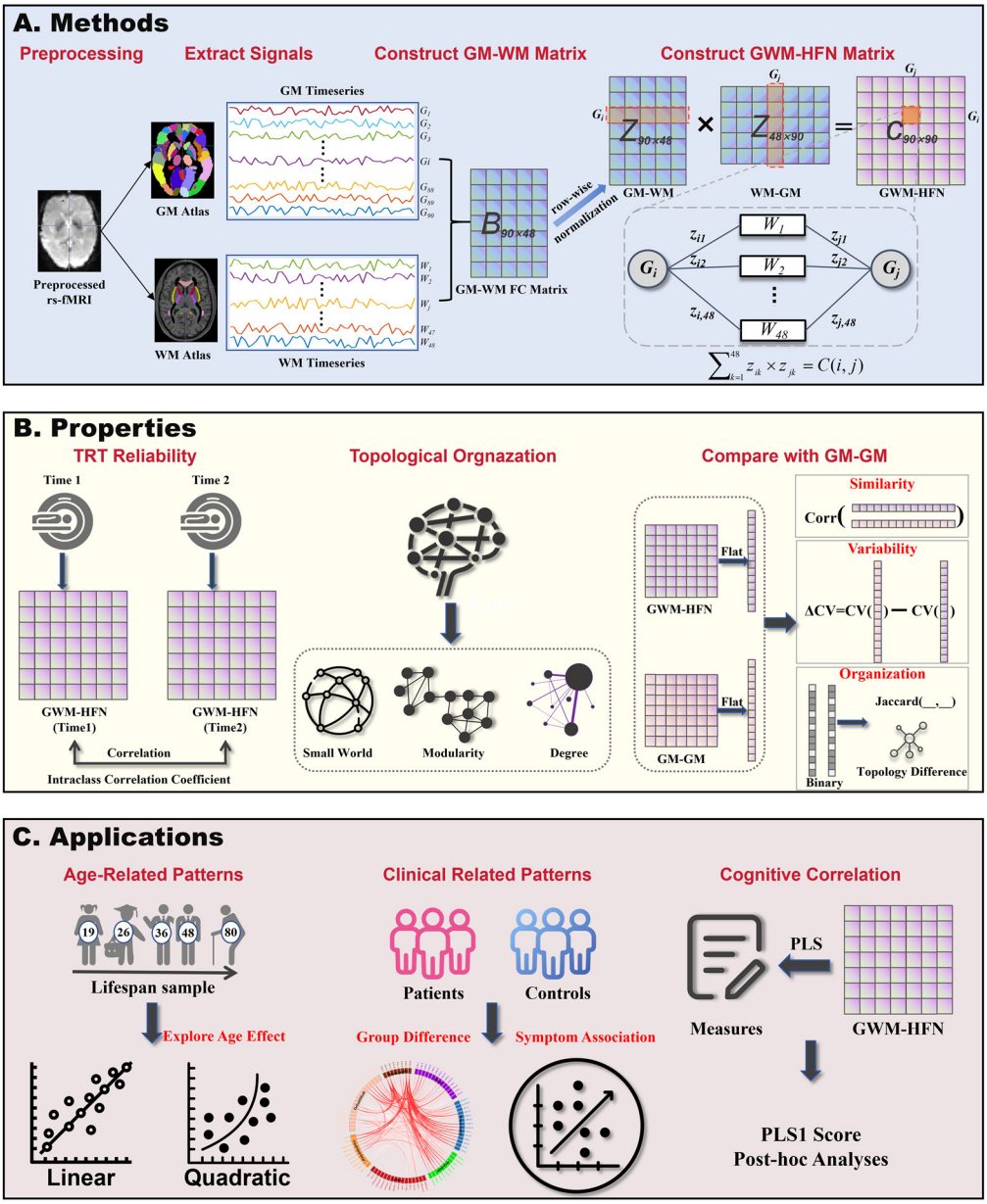

Figure 1. Schematic Overview of the Study Framework. (A) Development of the gray-white matter heterogeneous fusion network (GWM-HFN). This phase initiated with the extraction of gray matter (GM) and white matter (WM) signals from preprocessed rs-fMRI datasets to create a GM-WM connectivity matrix B. Following this, the values were standardized row-wise to generate a Z-score matrix, highlighting the relative interaction profile of each region within its connectivity framework. Ultimately, the covariance matrix C, which was obtained from Z, functioned as a GM FC matrix mediated by WM, also referred to as the GWM-HFN. (B) Analysis of GWM-HFN Characteristics. The research evaluated the test-retest reliability of the GWM-HFN network alongside its topological characteristics using graph theoretical metrics. Additionally, comparative assessments between GWM-HFN and conventional GM-GM connectivity networks were carried out. (C) Utilization of GWM-HFN. The practical relevance of the GWM-HFN was investigated across three areas. First, examining its age-related trends, which included both linear and quadratic effects; second, evaluating its use in clinical settings; and third, applying partial least squares (PLS) regression to assess its predictive ability for cognitive and behavioral outcomes.

2.2 Gray-White Matter Heterogeneous Fusion Network Patterns (SLIM Dataset)

For every one of the 570 younger healthy individuals (ages 17-27) from the SLIM dataset (baseline), we developed GWM-HFN and traditional GM-GM networks. Figure 2B illustrates the mean connectivity matrices at the group level for the constructed GWM-HFN and traditional GM-GM networks. Generally, the connectivity matrices revealed consistently higher intra-network connectivity among large-scale functional subnetworks (such as visual and frontal-parietal networks) and moderately strong inter-network connections, regardless of whether GWM-HFN or GM-GM was analyzed. Nevertheless, there is a distinct pattern indicating that GWM-HFN is predominantly stronger than GM-GM regarding both inter-network and intra-network connection strength. Detailed comparisons with the conventional GM-GM will follow later. These baseline findings indicate that GWM-HFN, which incorporates WM signals, could enhance our comprehension of long-range communication

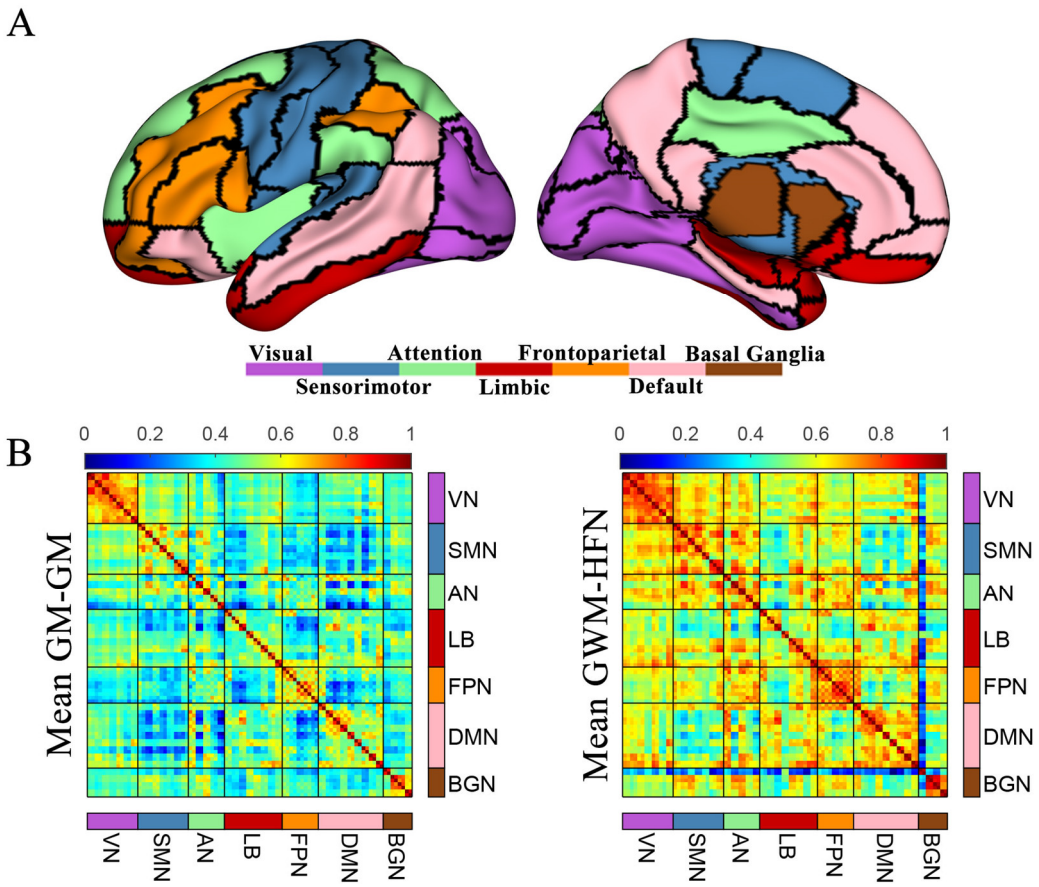

Figure 2. (A) A schematic representation of the division of 90 brain regions into seven large-scale networks; **(B)** Group-level mean GM-GM connectivity strength matrix (r-value matrix) and GWM-HFN connectivity strength matrix, both normalized to a range of 0–1 for comparability.

2.3. Short- and Long-Term TRT Reliability (BNU-3 and SLIM Datasets)

The BNU-3 dataset was used to assess short-term test-retest (TRT) reliability, with each participant undergoing three scanning sessions within a single day. In contrast, the SLIM dataset was employed to evaluate long-term TRT reliability. Participants in this dataset underwent up to three scanning sessions, although only a subset completed the second and third sessions. For the purposes of this study, only the first two time points—separated by an average interval of 304.14 days—were used to assess long-term TRT reliability.

As illustrated in Figures 3A and 3B, the GWM-HFN exhibited stable and consistent connectivity patterns across time points at the group level in both datasets. Group-averaged connectivity networks showed strong correlations across sessions, with a mean Pearson correlation of r=0.955 for short-term reliability (BNU-3) and r=0.897 for long-term reliability (SLIM). At the individual level, we also computed the Pearson correlation coefficients between connectivity matrices across different time points. In the SLIM dataset, the average correlation between the two time points was 0.37 (±0.13), as shown in the lower-right corner of Figure 3A. In the BNU-3 dataset, the average correlation across time points was approximately 0.53 ($r_{1,2} = 0.57; r_{1,3} = 0.52; r_{2,3} = 0.50$), as shown in the lower-right corner of Figure 3B.

We further quantified the TRT reliability of individual connections within the GWM-HFN utilizing intraclass correlation coefficient (ICC) measure. As shown in Figure 3C, the GWM-HFN exhibited a mean edge-wise ICC of 0.36 (±0.12) in the BNU-3 dataset, whereas the SLIM dataset demonstrated a mean edge-wise ICC of 0.20 (±0.08). These findings align with previous observations that long-term reliability is generally lower than short-term reliability, likely due to increased variability introduced by longer intervals between measurements (e.g., physiological changes and day-to-day fluctuations)[26,27].

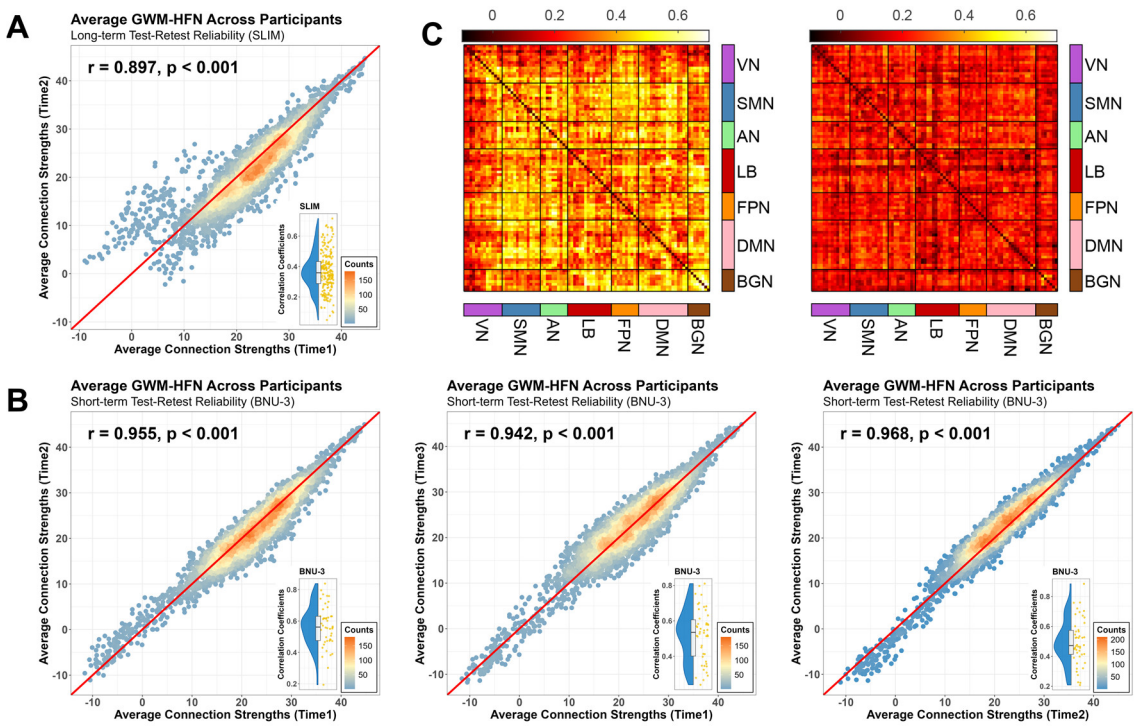

Figure 3. (A) Scatterplot of group-averaged gray-white matter heterogeneous fusion network (GWM-HFN) connectivity strengths between two time points in the SLIM dataset. The X-axis represents connectivity strengths at time point 1, while the Y-axis represents those at time point 2. (B) Scatterplots of group-averaged GWM-HFN connectivity strengths between each pair of three time points in the BNU-3 dataset. The X and Y axes correspond to connectivity strengths at the respective time points. For (A) and (B), the inset in the lower-right corner of each plot illustrates raincloud plots of correlation coefficients at the subject level for GWM-HFN across two time points. (C) Heatmaps of edge-level intraclass correlation coefficient (ICC) sparsity matrices, with the left panel depicting short-term test-retest reliability (TRT) and the right panel showing long-term ICC values.

2.4. Topological Organization of the GWM-HFN (SLIM dataset)

For the GWM-HFNs derived from the 570 younger healthy participants from the SLIM time1 dataset, we calculated a set of graph-based network measures across varying sparsity thresholds (0.10-0.34, step=0.01) to study their topological organization, including small-world organization, modularity architecture, degree distribution, and hubs.

2.4.1. Small-World Properties and Modularity

The GWM-HFN consistently demonstrated characteristics indicative of a classic small-world network configuration. This was evidenced by normalized clustering coefficients exceeding 1, alongside characteristic path lengths approximating 1, as illustrated in Figure 4A. Such properties suggest a

network topology that facilitates efficient information transfer and integration among disparate brain regions. Moreover, the modularity coefficient (Q) consistently remained above 0.3 across a wide threshold range (Figure 4B), suggesting that explicit WM inclusion produces well-segregated community structures that may capture local clustering mechanisms.

2.4.2. Hub Distribution and Degree

The degree distribution observed in the group-level mean GWM-HFN was best represented by an exponentially truncated power law model, achieving a high goodness-of-fit (R^2=0.959), as shown in Figure 4C. This particular form of degree distribution is indicative of the presence of highly connected regions, commonly referred to as hubs, within the GWM-HFN. Notably, 14 hub nodes were identified, distributed across the frontal, limbic, occipital, and temporal lobes (Figure 4D), emphasizing their pivotal roles in the brain's functional connectivity architecture.

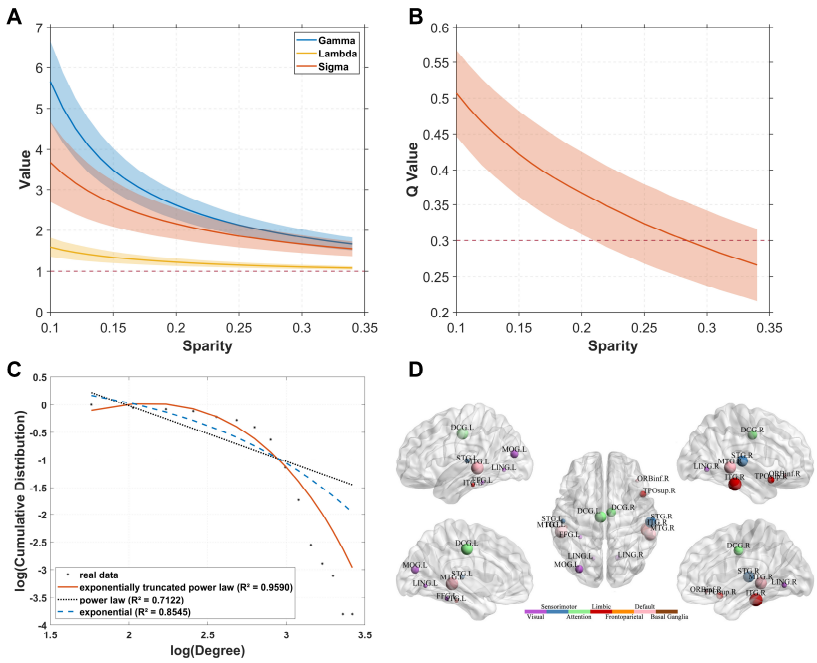

Figure 4. Topological Characterization of the Gray-White Matter Heterogeneous Fusion Network (GWM-HFN). (A) Small-world properties—sigma (σ), normalized clustering coefficient (γ), and normalized characteristic path length (λ)—of the GWM-HFN across a range of sparsity thresholds, presented as mean ± standard deviation. (B) Modularity coefficient (Q) of the GWM-HFN across varying sparsity thresholds, also shown as mean ± standard deviation, indicating robust modular organization. (C) Degree distribution of the group-averaged GWM-HFN, best fitted by an exponentially truncated power-law model, revealing the existence of highly connected brain regions. (D) Identification of 14 hub nodes within the group-averaged GWM-HFN, highlighting their central roles in the brain's functional connectivity architecture.

2.5. Comparison with Traditional GM-GM Networks (SLIM Dataset)

2.5.1. Similarity Assessment

To evaluate the added value of incorporating white matter in connectivity modeling, we compared the GWM-HFN with traditional GM-GM networks at the edge, network, and global levels using the SLIM dataset. At the edge level, the two network types exhibited strong similarity, with an average Pearson correlation coefficient of 0.77 (±0.038). As shown in Figure 5A, a representative participant's data revealed a high correlation between GWM-HFN and GM-GM connection strengths ($r = 0.743$). Nevertheless, this suggests that more than 40% of the variance remains unique to each network type. To better understand these differences, we identified the 5% of edges with the highest and lowest correlations between the two networks, illustrated in Figures 5B and 5C. Edges with low correlations were primarily intra-network connections within specific functional systems such as the VN, FPN, and DMN. In contrast, highly correlated edges were predominantly inter-network connections, especially between the BGN and other systems like the VN, SMN, LB, and DMN. This trend was consistent at the network level: inter-network correlations across large-scale functional networks were stronger (mean $r = 0.84$) than intra-network correlations (mean $r = 0.79$), as depicted in Figure 5D. At the global level, GWM-HFN and GM-GM connectivity profiles showed robust consistency across participants, with a global correlation coefficient of 0.87. These results underscore a substantial overlap between the two connectivity frameworks, while also revealing nuanced differences in how functional systems are represented.

2.5.2. Variability Assessment

To assess differences in individual variability between the GWM-HFN and traditional GM-GM networks, we calculated the coefficient of variation (CV) for each edge. At the edge level, 480 connections showed statistically significant differences in CV. Remarkably, 477 of these edges exhibited greater variability in the GWM-HFN, whereas only 3 showed higher variability in the GM-GM network. As shown in Figure 5E, these variable edges were predominantly associated with connections linking the basal ganglia network (BGN) and limbic system (LB) to other networks, especially involving the

hippocampus and caudate regions (Figure 5F).

To further examine the relationship between network similarity and variability, we stratified all 4,005 possible edges (calculated as 90 × 89 / 2) into three equal groups of 1,335 edges based on their similarity scores (i.e., Pearson correlation between GWM-HFN and GM-GM connectivity). A one-way ANOVA revealed significant variability differences among the three groups ($F(2,4002) = 37.02$, $p < 0.001$; Figure 5G). Notably, edges with greater similarity between the two networks exhibited smaller differences in variability ($r = -0.12$, $p = 3.70 \times 10^{-15}$; Figure 5H).

These findings suggest that the GWM-HFN captures a broader range of individual variability, potentially reflecting the added contribution of white matter connectivity. Moreover, higher similarity between GWM-HFN and GM-GM networks is associated with reduced variability differences, highlighting the unique yet complementary roles of gray and white matter in shaping functional brain networks.

2.5.3. Network Organization Assessment

To evaluate the organizational similarity between GWM-HFN and GM-GM networks, we computed Jaccard coefficients across a range of sparsity thresholds (0.01–0.50). The average coefficients ranged from 0.39 to 0.66, with values increasing at higher sparsity levels (Figure 5I), indicating greater structural alignment at higher network densities. At lower sparsity thresholds, notable discrepancies emerged, reflecting amplified structural differences between the two network types. This pattern was further nuanced across functional modules (Figure S1). Specifically, inter-network connections demonstrated lower baseline similarity, which progressively increased with sparsity, while intra-network connections showed higher baseline similarity but followed a U-shaped trajectory, reaching a minimum around 0.05 sparsity. These results suggest that white matter pathways introduce distinct network architectural features, particularly in sparse functional networks, emphasizing the complementary contributions of GWM-HFN connectivity to traditional gray matter-based analyses.

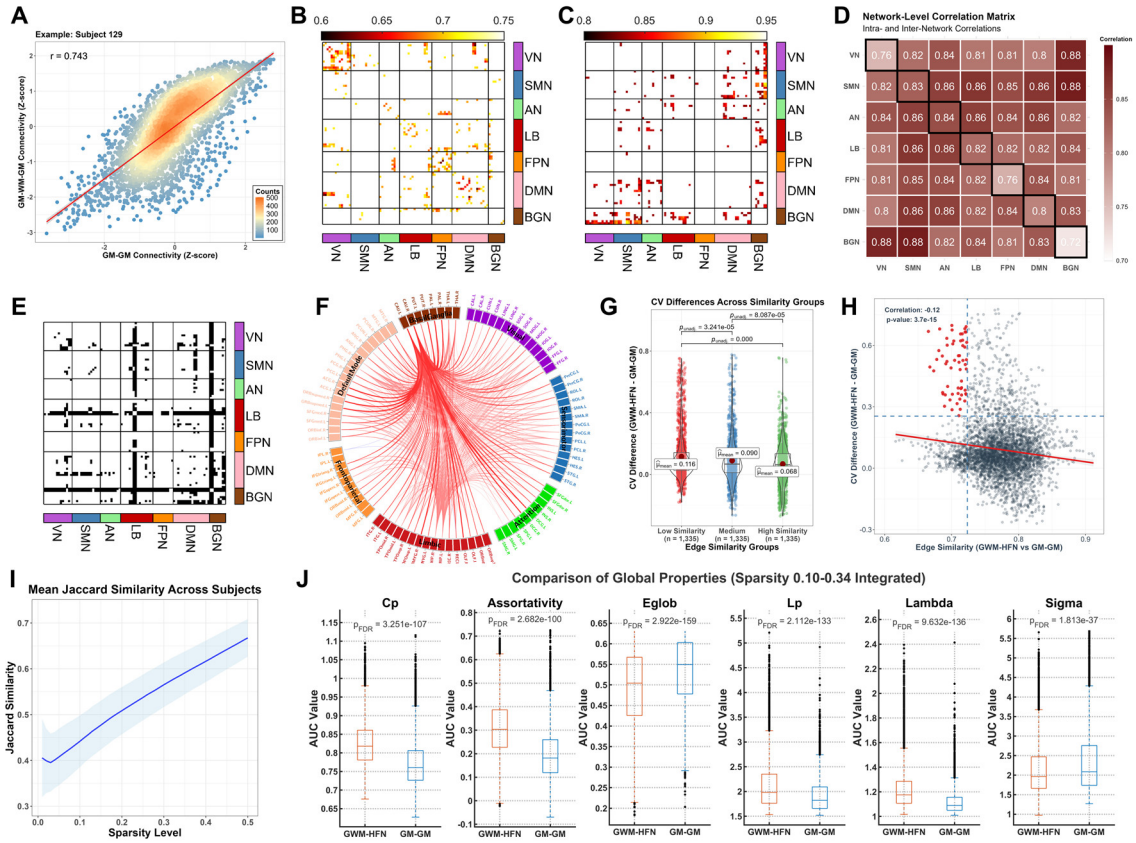

Figure 5. Comparative Analysis of GWM-HFN and GM-GM Networks. (A) Scatterplot illustrating the relationship between GWM-HFN and GM-GM connection strengths for a representative participant, showing a high correlation (r = 0.743). (B, C) Heatmaps highlighting edges with the lowest (<5th percentile) and highest (>95th percentile) correlations between the two network types, respectively. (D) Network-level correlation analysis revealing stronger inter-network correlations (mean r = 0.84) than intra-network correlations (mean r = 0.79) between GWM-HFN and GM-GM connectivity. (E) Binary matrix heatmap depicting edges with significant differences in coefficient of variation (CV) between the two networks. (F) Circular plot of these differential edges, where red lines represent greater variability in GWM-HFN, blue lines indicate higher variability in GM-GM, and line thickness corresponds to the magnitude of the difference. (G) Violin plot comparing CV differences across three edge groups (1,335 edges each) stratified by similarity, showing significant variability differences ($F(2,4002) = 37.02$, $p < 0.001$). (H) Scatterplot showing a negative correlation ($r = -0.12$, $p = 3.70 \times 10^{-15}$) between edge-level similarity and variability difference. (I) Line plot of average Jaccard coefficients across sparsity thresholds (0.01–0.50), with shaded regions representing standard deviation, demonstrating consistency across thresholds. (J) Box plots comparing the area under the curve (AUC) for global topological properties—including clustering coefficient, assortativity, characteristic path length, global efficiency, and small-worldness—across the 0.10–0.34 sparsity range, indicating significant differences between GWM-HFN and GM-GM networks.

To more comprehensively assess topological differences, we performed a graph-theoretical analysis using area under the curve (AUC) metrics calculated from the 0.10–0.34 sparsity range, with statistical

comparisons based on paired t-tests. Results revealed that GWM-HFN networks are topologically distinct, exhibiting enhanced modular segregation but reduced global integration compared to GM-GM networks. GWM-HFN networks showed significantly higher Clustering Coefficient (Cp) and Assortativity, reflecting increased local cohesiveness and node-type homogeneity (Figure 5J). These differences extended to regional levels, where Nodal Clustering Coefficient and Subgraph Centrality were significantly higher across numerous brain areas. Lower Participant Coefficient in GWM-HFN networks suggested stronger modular boundaries, implying that white matter-informed connectivity preserves distinct community structures more rigidly (Figure S2). In contrast, GWM-HFN networks demonstrated significantly longer Characteristic Path Lengths (Lp) and lower Global Efficiency (Eglob), consistent with reduced capacity for rapid and efficient global information transfer (Figure 5J). This was associated with reduced Small-Worldness (Sigma), reflecting a diminished balance between segregation and integration. While Betweenness Centrality was significantly elevated in many GWM-HFN nodes, indicating increased control over information flow, other metrics—including Degree, Eigenvector Centrality, PageRank Centrality, and Nodal Efficiency—exhibited bidirectional changes across brain regions, suggesting a complex reorganization of functional hubs and peripheral nodes (Figure S2). Collectively, these findings demonstrate that GWM-HFN networks encode a distinct functional topology, marked by heightened modularity and segregation but less efficient global integration, highlighting the neurobiological value of incorporating white matter pathways into functional connectome modeling.

2.6. Age-Related Patterns in GWM-HFN (SALD datasets)

Using the SALD datasets, which include a broad adult age range from 19 to 80 years, we examined how GWM-HFN connectivity evolves across the lifespan. Linear and quadratic regression models were applied to assess the relationship between age and connectivity strength, with head motion and sex controlled as covariates. At the global level, GWM-HFN connectivity showed a significant negative linear association with age ($r = -0.252$, $p < 0.001$; Figure 6A), while the quadratic term was not statistically significant ($p = 0.296$), indicating a predominantly linear age-related decline.

At the edge level, over half of all connections (2044 out of 4005; 51.04%) were significantly

modulated by age after FDR correction. Notably, 78.47% of these age-sensitive edges (1604 connections) exhibited negative linear associations, suggesting widespread weakening of GWM-HFN connectivity with aging. A smaller proportion (1.96%, 40 edges) showed positive linear trends, indicating a limited set of connections that strengthen over time (Figure 6B, left panel). In addition to linear effects, quadratic age-related patterns were identified in 400 edges (19.57%). Of these, 96% (384 edges) followed inverted U-shaped trajectories, peaking before declining, whereas 4% (16 edges) followed U-shaped curves with initial decline followed by later-life increases (Figure 6B, right panel). The average peak age for connections with significant quadratic effects was 33.84 years, suggesting a critical window of maximal GWM-HFN in early adulthood. At the large-scale functional network level, both linear and quadratic effects predominantly involved between-network connections (1728 vs. 316 edges). Specifically, as shown in Figure 6C, connections with significant linear age effects were primarily distributed among the LB, DMN, and SMN, while those with significant quadratic effects were mainly observed between the SMN, DMN, LB, and AN.

Finally, we observed a high correlation between GWM-HFN and traditional GM-GM connectivity across subjects (mean $r = 0.735$), which intensified with increasing age (Figure 6D). This finding suggests that the convergence between GWM-HFN and gray matter-based functional networks becomes more pronounced in older individuals.

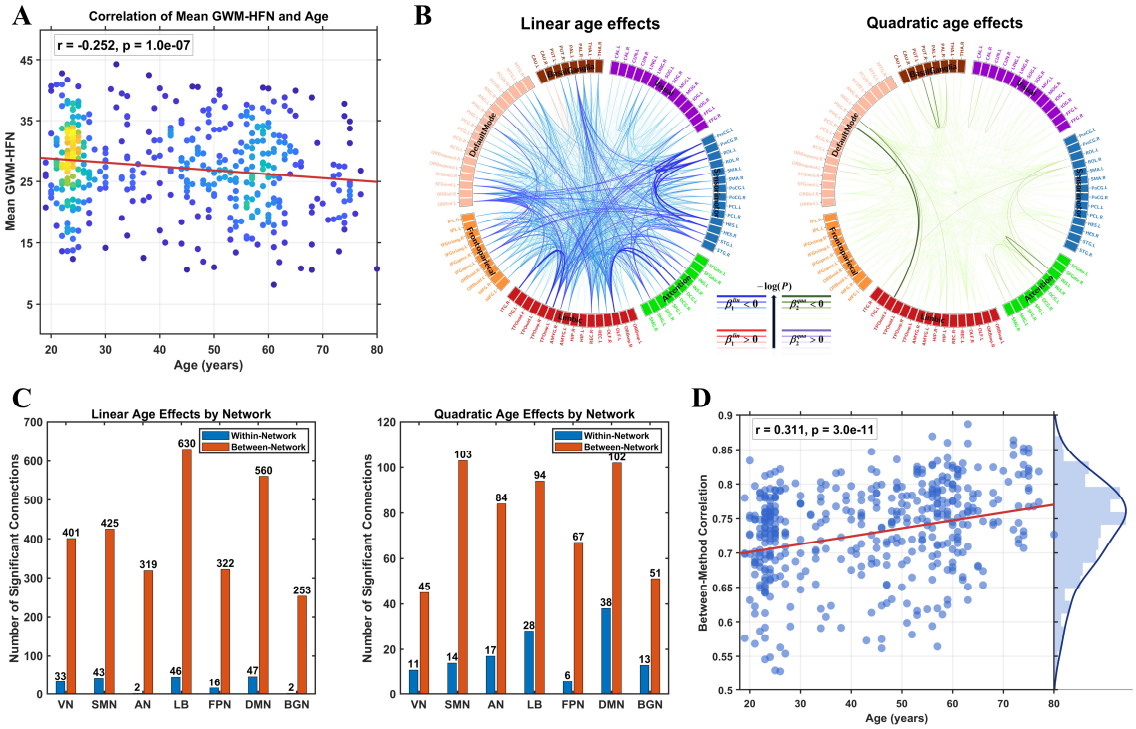

Figure 6. Age-Related Patterns of GWM-HFN Connectivity. (A) Scatter plot illustrating the negative linear correlation between mean GWM-HFN connectivity and age ($r = -0.252$, $p = 1.0 \times 10^{-07}$). Each dot corresponds to an individual participant, and the red line depicts the fitted linear regression. (B) Circular connectograms depicting edge-level age effects on GWM-HFN connectivity. Left panel: Linear effects—blue lines indicate negative correlations (connectivity decreases with age), while red lines indicate positive correlations (connectivity increases with age). Right panel: Quadratic effects—green lines represent inverted U-shaped relationships (connectivity increases then decreases), while purple lines denote U-shaped patterns (initial decline followed by increase). Line thickness represents the magnitude of age effects. Brain regions are color-coded according to their associated functional networks. (C) Bar plots quantifying the distribution of significant age effects across functional networks. Left panel: Number of linear age effects, showing a predominance of between-network changes. Right panel: Number of quadratic age effects, also revealing a majority of changes occurring between networks. (D) Scatter plot showing the positive correlation between age and the similarity of GWM-HFN and GM-GM connectivity patterns ($r = 0.311$, $p = 3.0\times 10^{-11}$). Blue dots represent individual participants, the red line shows the linear fit, and the marginal plot on the right illustrates the overall distribution of between-method correlations.

2.7. Clinical Relevance: Insights from Patient Cohorts

ASD was selected as the clinical example for this study due to extensive and well-documented evidence of white matter structural abnormalities and atypical brain functional networks in individuals with this neurodevelopmental condition[28–30]. These established neuropathological features provide a strong basis for investigating the clinical relevance of GWM-HFN connectivity. To assess this, we

constructed networks for individuals with ASD and TC individuals using the ABIDE-II dataset, a large-scale, multi-site repository that integrates neuroimaging data from diverse international cohorts. Prior to analysis, we applied the ComBat method for harmonization to minimize the impact of sites[31]. This technique effectively corrected for potential biases in GWM-HFN connectivity across the 13 contributing sites, as demonstrated by reduced differences in both mean and variance before and after harmonization (**Figure 7A**).

We first conducted group comparisons, controlling for age, sex, and mean FD as covariates. Results revealed that individuals with ASD exhibited significantly stronger global mean GWM-HFN connectivity compared to TC ($t = 2.055, p = 0.042$). In contrast, no significant differences were observed in mean GM-GM connectivity between the groups, as illustrated in **Figure 7B**. At the edge level, 323 GWM-HFN connections showed significant group differences, all indicating increased connectivity in the ASD group (**Figure 7C**). In comparison, the GM-GM connectivity network revealed only 106 significant edges, of which 102 also showed stronger connectivity in ASD. Remarkably, 80% (85 out of 106) of these significant GM-GM connections overlapped with the GWM-HFN connections (**Figures 7D & 7E**), underscoring the heightened sensitivity of GWM-HFN in detecting ASD-related alterations.

Subsequently, we examined whether these significant connections were predominantly intra-network or inter-network. For both GWM-HFN and GM-GM networks, inter-network connections were more prevalent. Notably, the BGN accounted for the highest number of significant connections in both intra- and inter-network analyses across both methods (**Figure 7F**).

Finally, we investigated whether the identified GWM-HFN connections were associated with the severity of autistic symptoms, as measured by the Autism Diagnostic Observation Schedule-Generic (ADOS-G). Specifically, we calculated the correlation between the total ADOS-G score (ADOS_G_TOTAL) and the mean connectivity strength of the identified GWM-HFN connections. Our analysis revealed a significant negative correlation between the mean GWM-HFN connectivity and the total ADOS-G score ($rho = -0.25, p = 0.0011$), as illustrated in **Figure 7G**.

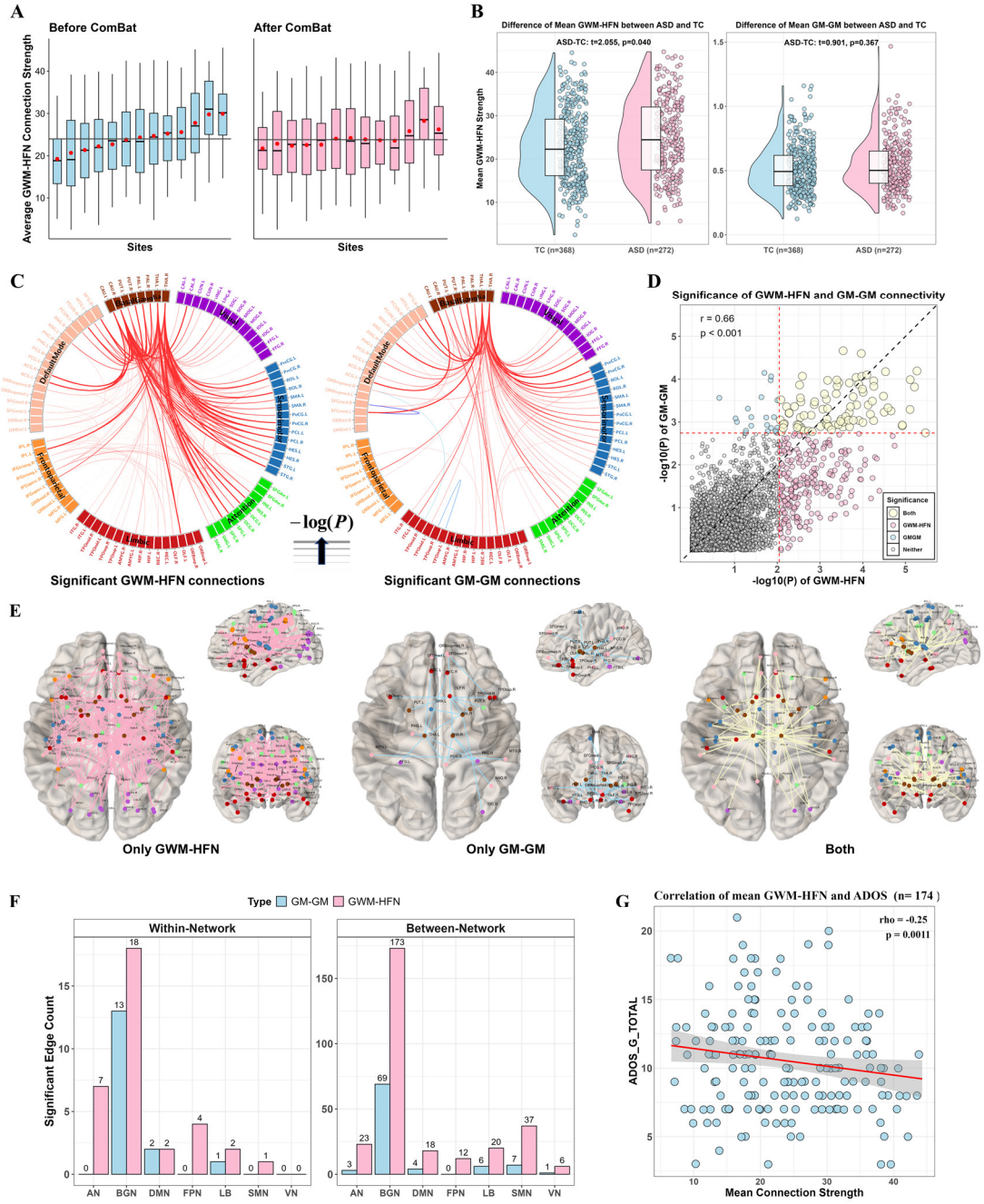

Figure 7. Comparative Analysis of GWM-HFN Connectivity Between ASD and TC Groups. (A) Boxplot illustrating the global mean GWM-HFN connectivity across 13 acquisition sites before and after harmonization. The red diamond indicates the mean connectivity within each site, while the gray line represents the overall mean connectivity across all sites. (B) Raincloud plot comparing the global-averaged GWM-HFN and GM-GM connectivity strengths between the ASD and TC groups. (C) Left panel: Brain network depicting the significantly different GWM-HFN connections identified between the ASD and TC groups, with all significant connections showing greater connectivity in the ASD group (ASD > TC), indicated by red. Right panel: Brain network illustrating the significantly different GM-GM connections identified between the ASD and TC groups, with the majority of connections exhibiting greater connectivity in the ASD group (ASD > TC), indicated by red. Connections showing decreased connectivity in the ASD group (ASD < TC) are indicated by blue. Line thickness corresponds to the

magnitude of the effect size. (D) Scatterplot comparing the p-values of group differences for GWM-HFN and GM-GM functional connections. The two red dashed lines indicate the threshold for significance after FDR correction ($P_{FDR} < 0.05$). Data points are color-coded based on the significance of the connection: light yellow for connections significant in both the GWM-HFN and GM-GM analyses, light red for connections significant only in the GWM-HFN analysis, and light blue for connections significant only in the GM-GM analysis. (E) Brain connectivity map visualizing connections that were significant only in the GWM-HFN analysis, significant only in the GM-GM analysis, and significant in both analyses. (F) Scatterplot showing the correlation between the mean strength of significant GWM-HFN differences and ADOS-G total scores. Spearman's rank correlation coefficient was used to quantify the strength of this association.

2.8. GWM-HFN Correlations with Cognitive and Behavioral Measures

The BGSP dataset included a broad array of behavioral and cognitive measures, enabling exploration of phenotypic correlates of GWM-HFN connectivity. To investigate these associations, we employed partial least squares (PLS) regression to evaluate whether GWM-HFN connectivity could explain interindividual differences in four cognitive-behavioral phenotypes: Shipley vocabulary score, matrix reasoning scores, and estimated IQ derived from both Shipley-Hartford T-scores and the OPIE3 formula.

Our analysis focused on the first PLS component (PLS1), which represents the linear combination of GWM-HFN connectivity features most strongly associated with the behavioral data. Using permutation testing, we found that PLS1 scores explained a significant proportion of variance in both the Shipley vocabulary task ($8.95\%, P_{permutation} = 0.0229$, **Figure 8A**) and the Shipley-Hartford estimated IQ ($9.09\%, P_{permutation} = 0.0186$, **Figure 8B**). However, no significant associations were found for the matrix reasoning score ($P_{permutation} = 0.728$) or IQ estimated using the OPIE3 formula ($P_{permutation} = 0.654$). To identify the connectivity patterns driving these effects, we examined the standardized PLS1 weights. Connections with absolute weights exceeding 3 standard deviations ($|z| > 3\sigma$) were selected for visualization. For the Shipley vocabulary task, significant weights were predominantly negative and localized within the default mode network (DMN), suggesting that lower DMN connectivity is linked to better vocabulary performance. Conversely, for the Shipley-Hartford estimated IQ, significant weights were primarily positive and observed between the DMN and the basal ganglia network (BGN), indicating that stronger DMN–BGN connectivity corresponds to higher IQ scores.

To further validate these associations, we applied the brain bias set (BBS) modeling method[32] to predict individual scores in the cognitive domains identified as significant in the PLS analysis. Results showed that GWM-HFN connectivity significantly predicted individual scores in the Shipley vocabulary task (mean $r = 0.0813, P_{permutation} = 0.0255$, Figure 8E), while no significant prediction was found for IQ estimated using the Shipley-Hartford T-scores. Finally, we calculated the contribution of each edge to the prediction of vocabulary scores and visualized those with the highest contributions (|z| > 3σ), as depicted in Figure 8F.

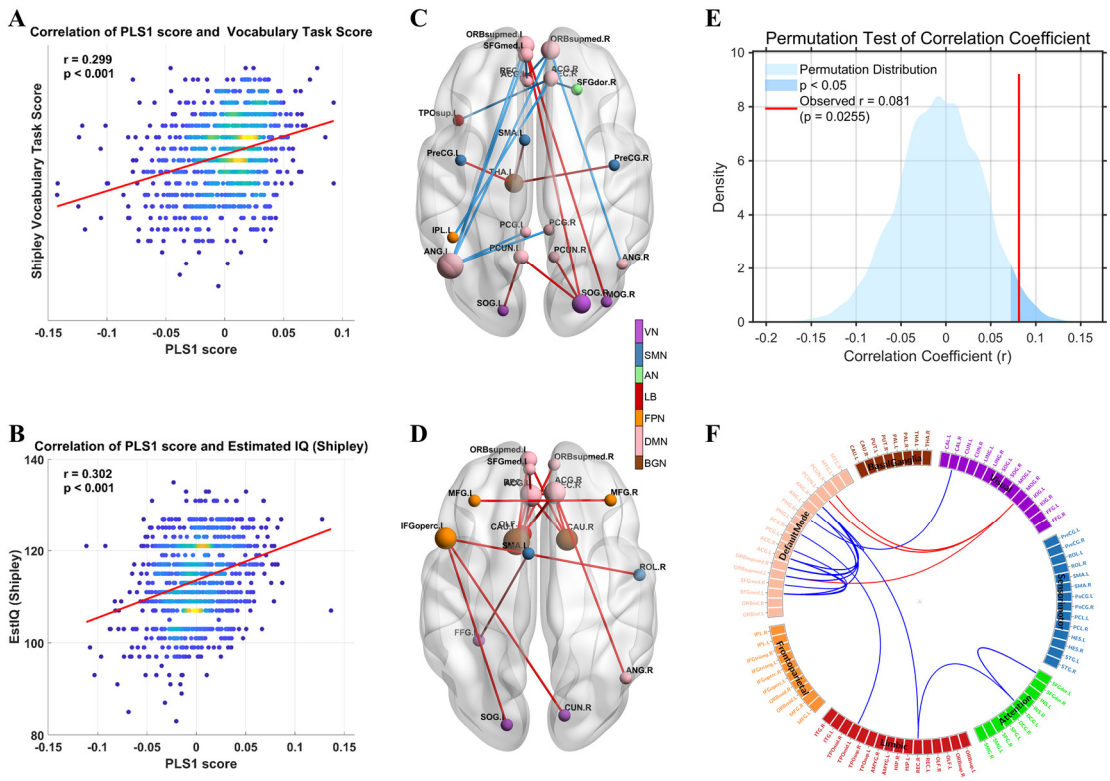

Figure 8. Association between GWM-HFN connectivity and Behavior and Cognition measures. (A) Correlation between PLS1 scores and the Shipley vocabulary task scores; (B) Correlation between PLS1 scores and the estimated IQ derived from Shipley-Hartford Age-Corrected T-Scores. (C) Brain visualization of connectivity patterns for the Shipley vocabulary task, displaying edges with absolute standardized PLS1 weights exceeding 3σ. (D) Brain visualization of connectivity patterns for the estimated IQ derived from Shipley-Hartford Age-Corrected T-Scores, displaying edges with absolute standardized PLS1 weights exceeding 3σ. (E) Density plot of 10,000 permutation tests for the correlation coefficient (r) between GWM-HFN connectivity and Shipley vocabulary task scores using the BBS modeling method. The blue curve represents the permutation distribution, with the shaded region indicating p < 0.05. The red vertical line marks the observed r = 0.0813(p = 0.0255). (F) Key connectivity patterns with absolute values exceeding 3σ. Positive weights are shown in red, and negative weights in blue.

3. Discussion

This study introduces and rigorously validates the GWM-HFN, a novel framework that reliably integrates WM BOLD signals into functional connectome analysis. Our multi-dataset validation demonstrates GWM-HFN's robust test-retest reliability, distinct topological features, and relevance in capturing age-related and clinical alterations. Such comprehensive characterization across reliability, topology, and diverse applications addresses a critical need in the evolving field of unified GM-WM functional connectomics, where extensive validation of emerging models[22,23] is still developing. By providing a validated means to incorporate WM's functional contributions, GWM-HFN directly challenges the traditional GM-centric view in neuroimaging[2,7]. Specifically, its GM-centered representation, derived from GM-WM covariance, overcomes limitations of WM-only approaches[12,16] and bipartite GM-WM models that hinder conventional global network analyses due to absent closed-loop interactions [22]. GWM-HFN therefore offers a more holistic and interpretable model of whole-brain functional architecture, significantly advancing our capacity to map complex neural communication.

3.1 Reliability of GWM-HFN in the Context of Resting-State fMRI

A cornerstone of establishing the GWM-HFN framework's utility lies in its methodological viability, particularly its test-retest reliability. Our analyses yielded mean edge-wise ICCs of approximately 0.36 for short-term (BNU-3 dataset) and 0.20 for long-term (SLIM dataset) GWM-HFN connectivity. According to benchmarks such as those proposed by Landis and Koch[33], these ICCs position GWM-HFN reliability in the 'fair' (ICC = 0.21–0.40) and 'slight' to 'fair' (ICC ≈ 0.20) categories, respectively. These values must be interpreted within the challenging context of rs-fMRI research, where achieving high test-retest stability for any individual FC measure is non-trivial due to inherent physiological noise, ongoing unconstrained cognitive processes, and cross-study analytical variability[26,27].

Indeed, the observed ICCs for GWM-HFN are within the spectrum reported for many GM-based rs-fMRI connectivities[26]. The assessment of reliability in methodologies incorporating WM signals is an area of active development. For instance, Wang et al. investigated the robustness and reliability of direct WM functional connectivity[34], finding that while static FC in GM networks was stronger than in WM

networks, WM networks exhibited greater dynamism. Their study also reported a range of ICC values for WM static FC, underscoring the variability inherent in these measures but affirming that WM fMRI signals contain rich and analyzable spatiotemporal information. The GWM-HFN approach, by deriving connectivity from the covariance of GM regions' interaction profiles with WM tracts, aims to capture stable patterns of shared WM pathway utilization. This differs from direct WM-WM FC and may thus possess distinct reliability characteristics, potentially benefiting from its integrative nature which is less reliant on the amplitude of WM BOLD signals that are typically lower and possess different noise signatures than GM[10,11].

Furthermore, the pursuit of enhanced reliability in WM functional analyses underscores the critical importance of standardized and optimized preprocessing pipelines. As highlighted by the development of specialized toolboxes like WhiFuN[35], which incorporate WM-specific preprocessing steps to minimize GM signal contamination and optimize WM signal extraction, the field is moving towards more rigorous data handling. Such standardized approaches, coupled with robust quality control, are anticipated to improve the consistency and reproducibility of findings derived from WM BOLD signals. Therefore, the 'fair' reliability demonstrated by GWM-HFN, achieved through its specific analytical pipeline, is a crucial validation. It provides a necessary foundation for employing GWM-HFN in longitudinal studies and for investigating its potential in biomarker development where consistent tracking of individual differences is paramount[10], especially as evidence mounts for the reliable detection of meaningful, neurally-related activity in WM[13,14].

3.2 Distinct Topological Organization of WM-Mediated Functional Networks

The GWM-HFN framework not only demonstrates reliability but also unveils a unique topological signature for WM-mediated functional networks. These networks inherently possess characteristics of efficient organization, such as small-worldness, modularity, and hub structures, as established by our graph-theoretical analyses. More critically, when contrasted with conventional GM-GM networks, GWM-HFNs exhibit a distinct profile: enhanced functional segregation alongside reduced global integration efficiency. This topological shift is a direct consequence of the GWM-HFN methodology,

which defines GM-GM functional links based on their shared covariance profiles with WM tracts. Such an approach naturally groups GM regions that functionally 'resonate' with the same WM pathways, thereby strengthening intra-modular cohesion and revealing a functional architecture more explicitly sculpted by the brain's WM scaffolding[36–38]. The resulting increase in modularity and local clustering suggests that GWM-HFN can delineate functional communities whose integrity is fundamentally tied to specific WM conduits.

The observed reduction in global efficiency and increased path length in GWM-HFNs, relative to GM-GM networks, likely signifies the multi-step nature of WM-mediated communication (GM-WM-GM paths) versus potentially more direct GM-GM BOLD synchrony. This implies that while WM pathways facilitate specific and organized communication, the overall information transfer across the entire GWM-HFN might appear less direct or rapid when primarily channeled through these anatomically constrained routes[22,23]. This trade-off results in a modified small-world architecture, potentially favoring specialized processing within modules at the cost of global broadcasting efficiency. Furthermore, the GWM-HFN framework reshapes the functional importance of nodes; the elevated betweenness centrality of certain GWM-HFN hubs suggests they act as critical control points for inter-modular communication specifically within this WM-mediated system, distinct from hubs identified in GM-GM networks that may simply reflect high overall synchrony. Thus, the topological characteristics of GWM-HFN provide a more mechanistic view of functional organization, emphasizing how WM pathways structure and constrain neural communication.

3.3 Complementary Insights Beyond Conventional GM-GM Connectivity

While the GWM-HFN framework introduces a novel perspective by incorporating WM signals, its relationship with traditional GM-GM functional connectivity provides crucial context. Our findings indicate a considerable overlap (mean edge-level $r \approx 0.77$, SLIM dataset), affirming that GWM-HFN captures fundamental patterns of synchronous neural activity. However, the more than 40% of unique variance captured by GWM-HFN underscores its capacity to reveal aspects of functional organization not apparent in GM-only analyses. For instance, the observation that GWM-HFN diverges more from

GM-GM connectivity for intra-network connections (within VN, FPN, DMN) than for inter-network connections suggests a particular strength of GWM-HFN in elucidating how WM pathways shape the internal coherence and communication dynamics *within* these large-scale systems, potentially reflecting the influence of specific tracts that are critical for segregated processing. In contrast, the stronger concordance for inter-network connectivity, especially involving the basal ganglia, may indicate that broader, more widespread synchrony between diverse systems is robustly captured by both approaches.

A key contribution of GWM-HFN lies in its markedly enhanced sensitivity to inter-individual variability. The finding that nearly all significantly differing connections exhibited greater CV in GWM-HFN—particularly those involving the basal ganglia and limbic system—points beyond mere methodological divergence. This heightened variability likely taps into genuine biological differences in individuals' WM architecture, its microstructural integrity (potentially impacting BOLD signal characteristics in WM), and the efficiency or preferred routes of WM pathway utilization[39–41]. Such sensitivity is paramount for fields like developmental neuroscience and clinical research, where understanding individual trajectories and susceptibility is key[42]. The observation that higher similarity between GWM-HFN and GM-GM networks correlates with reduced variability differences further suggests that where GWM-HFN most diverges, it captures the most distinct individual-specific information related to WM contributions.

These differences in captured variance and sensitivity to individual differences are also reflected in the distinct network topology of GWM-HFN compared to GM-GM networks, as detailed previously (enhanced modular segregation and reduced global integration efficiency). Such topological distinctions are a natural consequence of a network model that explicitly accounts for WM-mediated interactions, aligning with emerging perspectives that WM signals actively contribute to the organization and potential 'rewiring' of GM functional communities[24]. Thus, GWM-HFN provides not just a similar picture to GM-GM networks but a complementary one, enriched by the functional information carried by WM pathways and offering a more nuanced understanding of brain-wide communication.

3.4 Age-Related Decline and Reorganization of GWM-HFN Connectivity

Applying the GWM-HFN framework across the adult lifespan (SALD dataset) revealed significant age-related dynamics, predominantly characterized by a linear decline in global mean connectivity strength. This overarching negative trajectory aligns well with the established literature documenting widespread age-related degradation in both structural WM integrity[43,44] and conventional GM functional connectivity[5]. It also resonates with findings from related WM-GM network models, such as the reduced global efficiency observed with increasing age in bipartite WM-GM networks[22]. This suggests that the efficiency or strength of WM-mediated functional communication pathways, as captured by GWM-HFN, undergoes a general decline with advancing age.

Beyond this global trend, GWM-HFN demonstrated sensitivity to more complex, edge-specific age trajectories. While the majority of affected connections exhibited linear decreases, reinforcing the theme of age-related weakening, a notable subset displayed inverted U-shaped quadratic patterns. These connections typically peaked in early adulthood (mean peak age ~34 years) before declining. The complexity of WM aging is further highlighted by recent studies that reported both U-shaped patterns in static WM network connectivity strength and inverted U-shapes in the temporal variability of WM-GM connectivity across the lifespan[20]. This non-linear pattern is particularly compelling, as this peak age roughly coincides with the culmination of protracted maturation processes for certain cognitive functions and for WM microstructural properties, such as myelination[45]. The GWM-HFN may thus be capturing a critical window of maximal efficiency in WM-mediated functional communication during early to middle adulthood, followed by senescence potentially linked to the known microstructural deterioration of WM pathways later in life[44]. The prevalence of these non-linear effects, particularly in between-network connections involving systems like the SMN, DMN, LB, and AN, highlights the differential aging of specific long-range communication routes mediated by WM.

Intriguingly, our findings (SALD dataset) also indicated that GWM-HFN and traditional GM-GM connectivity patterns become significantly more similar with advancing age. This convergence could reflect several underlying processes. One possibility is age-related neural dedifferentiation, where diminished functional specialization of brain networks[46,47] blurs the distinctions between connectivity reflecting direct GM synchrony and WM-mediated interactions, perhaps due to reduced specificity of

WM-guided pathways or compensatory, more diffuse brain activity[48]. Alternatively, a 'shared vulnerability' scenario might explain this convergence, whereby common aging mechanisms like vascular or metabolic decline, and diffuse microstructural wear in both GM and WM[22,43,44], could globally degrade both direct GM coupling and WM-pathway integrity, causing their functional signatures to appear more alike. Disentangling these potential contributors requires further research, but the GWM-HFN's capacity to capture this age-related shift in network relationships, alongside broader linear declines and nuanced non-linear trajectories, highlights its value in comprehensively studying functional brain aging and the evolving role of WM-mediated communication.

3.5 GWM-HFN Reveals Altered Connectivity in Autism Spectrum Disorder

This observed GWM-HFN functional hyperconnectivity likely relates to the atypical WM neurodevelopment and microstructure frequently reported in ASD[49,50]. While diffusion MRI studies often indicate reduced microstructural integrity (e.g., lower FA) across widespread WM tracts[51,52], and morphometric analyses show heterogeneity but potential aggregation of volume reductions in common pathways[53], the relationship between these structural characteristics and functional connectivity is intricate. The functional hyperconnectivity captured by GWM-HFN might signify compensatory mechanisms attempting to overcome less efficient signaling along structurally atypical pathways, or perhaps reflect altered excitatory/inhibitory balances specific to WM-mediated communication routes. The prominent involvement of BGN connections in our GWM-HFN findings aligns with reports of altered structural network topology involving the BGN even in preschool ASD[54], hinting at early developmental atypicalities in cortico-striatal circuits relevant to ASD symptomatology[55,56].

Crucially, the clinical relevance of these GWM-HFN alterations was substantiated by a significant negative correlation between the mean hyperconnectivity strength and total ADOS-G scores. This complex relationship (greater GWM-HFN hyperconnectivity associating with less severe symptoms) underscores the heterogeneity within ASD[51,53] and may reflect varying individual profiles of underlying pathology versus compensatory functional adjustments. Further research is needed to explore this connection across different symptom domains and developmental stages[52].

While our current study focused on ASD, the established vulnerability of WM pathways across a range of psychiatric disorders[39] suggests that sensitive functional probes like GWM-HFN could be

valuable more broadly. For ASD specifically, GWM-HFN's ability to detect robust functional alterations potentially missed by GM-GM analysis, coupled with its association with clinical severity, highlights its promise for complementing structural MRI and advancing our understanding of WM network dysfunction in this complex condition.

3.6 Linking GWM-HFN Connectivity to Individual Differences in Cognitive Performance

The functional significance of GWM-HFN was further underscored by its ability to explain interindividual variance in cognitive performance within the BGSP dataset. Initial PLS regression analyses revealed that GWM-HFN connectivity patterns were significantly associated with Shipley vocabulary scores and Shipley-Hartford estimated IQ. The dominant PLS component linked vocabulary performance primarily to negative connectivity weights within the DMN, consistent with the DMN's established role in semantic processing and language comprehension[57–59]. Higher estimated IQ, conversely, correlated with positive connectivity weights predominantly between the DMN and the BGN, aligning with literature implicating DMN-BGN interactions in higher-order cognitive control and executive functions[60,61].

To more rigorously test these brain-behavior relationships at an individual level, we employed the BBS modeling method, an approach designed to assess the predictive capacity of connectomic features for individual phenotypes[32]. The BBS method, as applied here, typically involves training a model on a subset of participants' connectivity data (often after dimensionality reduction) to predict behavioral scores in unseen individuals, with significance assessed through cross-validation and permutation testing. Our application of BBS modeling provided crucial nuanced validation: GWM-HFN connectivity significantly predicted individual Shipley vocabulary scores, identifying specific edge contributions. This robust individual-level prediction for vocabulary, surviving cross-validation, strongly suggests that certain WM-mediated functional pathways captured by GWM-HFN are indeed tightly linked to this specific cognitive skill.

Interestingly, while the initial PLS analysis indicated an association with Shipley-Hartford estimated IQ, this did not translate into significant individual-level prediction under the BBS framework. This

divergence is informative. PLS identifies broad patterns of covariance at the group level, whereas BBS provides a stricter test of individualized predictive utility. The lack of significant IQ prediction via BBS could suggest that either the true effect size for this particular IQ measure, while detectable by PLS, is insufficient for robust individual prediction with the current GWM-HFN feature set, or that the relationship between GWM-HFN connectivity and this IQ estimate is more complex and perhaps less directly linear than that observed for vocabulary. Sripada et al. themselves discuss how resting-state connectomes contribute to inter-individual variation[32]; it's plausible that GWM-HFN features relevant to IQ are more diffusely represented or interact in a manner not fully captured by the specific BBS implementation used. Nevertheless, the successful individual prediction of vocabulary scores via GWM-HFN strongly indicates that this framework captures behaviorally relevant variance tied to specific WM-mediated communication pathways, highlighting its potential beyond group-level associations and underscoring that WM functional signals, as integrated by GWM-HFN, are indeed meaningfully related to cognitive function.

3.7 Limitations

Several limitations should be acknowledged when interpreting these findings. First, while we utilized longitudinal data for reliability assessment, the ageing and clinical analyses were primarily cross-sectional, precluding definitive inferences about developmental trajectories or causal relationships between network changes and clinical status. Future longitudinal studies employing GWM-HFN are warranted. Second, the BOLD signal in WM is inherently weaker and potentially more susceptible to physiological noise and partial volume effects than in GM. Although rigorous preprocessing steps, including WM-specific smoothing and nuisance regression strategies, were implemented, residual influences cannot be entirely excluded[35]. Continued methodological refinement for optimizing WM signal extraction and denoising remains important[10]. Third, our analysis focused on static functional connectivity. Exploring the dynamic fluctuations of GWM-HFN connectivity and its interplay with dynamic GM connectivity could offer further insights into how WM shapes transient neural coordination[20]. Finally, the choice of specific GM (AAL) and WM (JHU-ICBM 48) atlases inevitably influences the results; replication using different parcellation schemes would strengthen the

generalizability of our findings[62]. The GWM-HFN construction itself, based on the covariance of GM-WM profiles, represents one specific approach to integrating heterogeneous signals; comparing it with alternative fusion strategies will be valuable future work.

3.8 Conclusion

In conclusion, this study introduces and comprehensively validates the GWM-HFN as a reliable and neurobiologically insightful approach that transcends the traditional GM-centric view by explicitly integrating WM functional signals. Our findings robustly demonstrate that GWM-HFN not only captures a distinct topological organization reflecting WM structural constraints[36,38] but also exhibits heightened sensitivity to inter-individual variability, alongside significant relevance to lifespan changes, clinical conditions like ASD, and cognitive performance. By providing a validated novel lens on WM-mediated functional communication, the GWM-HFN framework offers a critical advancement in bridging structural and functional connectomics. It thereby encourages a more holistic understanding of brain-wide communication, paving the way for refined investigations into the integral role of white matter in shaping the human connectome in both health and disease

4. Methods and Materials

4.1. Datasets

To comprehensively evaluate the constructed GM-WM-GM networks, we employed several independent datasets and conducted a systematic investigation from multiple perspectives. These analyses aimed to assess the networks' test-retest (TRT) reliability, elucidate their organizational principles, compare them with traditional GM-GM networks, and examine their associations with aging trajectories, clinical relevance, and behavioral and cognitive correlates.

Specifically, the Southwest University Longitudinal Imaging Multimodal (SLIM) dataset (http://dx.doi.org/10.15387/fcp_indi.retro.slim) was employed to investigate long-term TRT reliability and network topology, while the Beijing Normal University (BNU-3) dataset (http://dx.doi.org/10.15387/fcp_indi.corr.bnu3) was used to assess short-term TRT reliability. The Southwest University Adult Lifespan (SALD) dataset (https://fcon_1000.projects.nitrc.org/indi/retro/sald.html) and Chinese Human Connectome Project (CHCP) dataset (https://doi.org/10.11922/sciencedb.01374) were utilized to examine age-related trajectories in GM-WM-GM networks. The Autism Brain Imaging Data Exchange II (ABIDE-II) project (https://fcon_1000.projects.nitrc.org/indi/abide/abide_II.html) was analyzed to assess the clinical relevance of these networks. The Brain Genomics Superstruct Project (BGSP) was used to examine Behavioral and Cognitive Correlates of GM-WM-GM Networks. For a detailed description of these datasets, please refer to the Supplementary Materials (see "Study Datasets" section). **Table S1** provides a summary of the demographic details for each dataset.

4.2. Neuroimaging Preprocessing

Functional MRI images in all the datasets underwent the same analytical pipeline to construct GM-WM-GM networks unless stated otherwise.

All acquired images were subjected to preprocessing using a combination of the SPM12 toolbox (http://www.fil.ion.ucl.ac.uk/spm/software/spm12), DPARSF (http://rfmri.org/DPARSF) toolboxes. The preprocessing steps involved in this study were described extensively in the Supplementary Materials.

Briefly, the individual T1 images were segmented into WM, GM, and cerebrospinal fluid (CSF) using SPM12's New Segment algorithm and then normalized to the Montreal Neurological Institute (MNI) template. The rs-fMRI were removed the initial several time points, corrected for slice timing and head motion effects, and co-registered with the anatomical image. Subsequently, 24 motion-related parameters, the mean CSF signal and motion spikes were regressed out. The data were detrended and temporally filtered with a passband frequency of 0.01 - 0.10 Hz. Then, spatial smoothing was performed separately in the WM and GM using a kernel with 4 mm full-width half-maximum (FWHM). Finally, the processed images were normalized to the standard MNI template and resampled to 3 mm^3 voxels.

A manual quality control procedure was performed after preprocessing. The following criteria were used to assess data quality: (1) successful generation of all preprocessed results, (2) mean framewise displacement (FD) below 0.2 mm, and (3) visual inspection confirming satisfactory spatial normalization.

4.3. Construction of GWM-HFN Functional Connectome

As depicted in Figure 1, using the widely recognized AAL and JHU-ICBM 48 atlases, time series were extracted from 90 cortical GM regions (denoted as $g_i, i = 1, 2, ..., 90$) and 48 WM fiber bundles (denoted as $w_j, j = 1, 2, ..., 48$), derived from preprocessed functional imaging data. A 90×48 GM-WM functional correlation matrix was computed, representing the interaction between GM regions and WM tracts. In graph-theoretical terms, this GM-WM correlation matrix forms a bipartite graph $\mathcal{G} = \{G, W, E, B\}$, consisting of two distinct sets of nodes ($g_i \in G, w_j \in W$) where edges only connect nodes from different groups (with *E* representing the set of edges and *B* representing the edge weights). The lack of within-group connections (i.e., no WM-WM or GM-GM links) results in the absence of closed triangular paths, which complicates the evaluation of important network properties such as global efficiency[21]. To overcome this limitation, we propose a novel method that projects the original bipartite GM-WM network into a weighted unipartite network where only GM nodes are explicit, and WM nodes are implicit—referred to as the GWM-HFN.

Specifically, for each participant, the GM-WM correlation matrix (denoted as $B = (b_{ij})_{90\times48}$) is a 90 ×48 matrix where each row represents the functional connectivity of a GM region with multiple WM

regions. To account for variability in connectivity strength and ensure comparability across different GM regions, we applied row-wise Z-score normalization to ***B***, to normalize for overall connectivity strength differences across GM regions, yielding a normalized matrix ***Z***. This normalization is grounded in the biological principle that GM regions exhibit different levels of overall connectivity. By standardizing these values, the analysis emphasizes how each region interacts relative to its own connectivity profile, offering a clearer representation of the brain's functional organization. Next, we computed the covariance matrix ***C*** of ***Z'*** to represent the functional connectivity between GM regions mediated by WM pathways. Each element of the resulting 90×90 matrix $C = \left(c_{ij}\right)_{90\times 90} = Z \cdot Z'$ quantifies the communication strength between cortical region **i** and cortical region **j** via shared WM connections. Thus, ***C*** serves as a GM FC matrix mediated by WM, also known as the GWM-HFN FC. This approach highlights the relative FC between GM regions, allowing for the detection of subtle interactions while accounting for variations in connectivity magnitude. It facilitates deeper insights into network properties and the investigation of clinically relevant connectivity changes.

4.4. Test–Retest Reliability Analysis (BNU-3 and SLIM Datasets)

To evaluate the reliability of GWM-HFN FC, both short-term and long-term TRT reliability were assessed using the SLIM and BNU-3 datasets, respectively. First, we calculated the correlation between connectivity matrices at different time points at the individual subject level (e.g., the correlation between connectivity matrices at time 1 and time 2) and subsequently averaged these correlation coefficients at the group level. Furthermore, the ICC was used to quantify both short-term and long-term TRT reliability of GWM-HFN. A two-way random-effects model for single-measure agreement, ICC(2, 1), was employed, accounting for both individual variability and measurement consistency across time. Formally, for each edge in the GWM-HFN, the ICC was calculated as:

$$ICC(2,1) = \frac{MS_b - MS_r}{MS_b + (k-1)MS_r + k(MS_e - MS_r)/n} \tag{1}$$

where MS_b is the mean square between subjects, MS_r is the mean square between measurements (time points), MSe is the mean square error, k is the number of scans per subject (2 for SLIM dataset and 3 for BNU-3), and n is the number of subjects. This formula enables the evaluation of GWM-HFN functional

connectivity reliability across time points.

4.5. Topological Analysis of GWM-HFN (SLIM Dataset)

Before analyzing the topological properties of the GWM-HFN, a sparsity-based thresholding procedure was applied to convert the weighted networks into binary representations. Sparsity is defined as the ratio of actual edges to the maximum possible edges in the network. By applying subject-specific thresholds, this procedure ensures a consistent number of edges across participants and sessions under different analytical approaches. Given the absence of a definitive sparsity standard, we adopted a range of [0.10, 0.34] with an interval of 0.01, following the default settings in DPABINet[63]. This range ensures that the resulting binary networks remain both sparse and estimable for small-world analysis. Subsequently, various graph-based network measures, including small-world properties, modularity, and degree, were calculated using the DPABINet toolbox. Detailed formulas and interpretations of these measures are available in the relevant literature[64]. For this analysis, we utilized the SLIM time1 dataset.

Small world Organization

Firstly, to determine whether the GWM-HFN exhibits small-world properties, commonly observed in brain networks, we calculated key small-world metrics such as the clustering coefficient and characteristic path length for each subject's connectivity network. These global measures were normalized by comparing them to the mean values of 100 randomly rewired networks, generated while preserving the degree distribution of the original networks. A network is considered to exhibit small-world properties if it shows a normalized clustering coefficient (γ) greater than 1 and a normalized characteristic path length (λ) close to 1, indicating local clustering and global efficiency comparable to random networks[65].

Modularity

We also calculated the modularity coefficient Q, which quantifies the degree to which a network can be divided into distinct modules or communities. The Q value is between 0~1 and the real network modularity function value is generally between 0.3~0.7[66]. Higher values of Q indicate a more pronounced

modular structure, suggesting that the network is composed of tightly connected clusters with relatively sparse connections between them.

Degree Distribution and Hubs

To investigate the roles of individual nodes in GWM-HFN, we calculated the nodal degree for GWM-HFN across a range of sparsity thresholds. In the context of brain networks, degree distributions often follow power-law-like distributions, suggesting a scale-free organization[67]. Therefore, after averaging the nodal degree across participants and sparsity levels, we applied different models (power law, exponential, and exponentially truncated power law) to fit the degree distribution of the GWM-HFN. Regions with average nodal degrees in the top 15% were classified as hubs.

4.6. Comparison of GWM-HFN and GM-GM Networks (SLIM Dataset)

The GM-GM network captures direct functional interactions between GM regions, whereas the GWM-HFN incorporates WM pathways, thereby representing a more complex and indirect connectivity structure. It is crucial to determine whether the GWM-HFN provides unique information that offers additional value beyond the GM-GM network. To this end, we conducted a series of analyses across multiple dimensions, including edge-level correlations, population variability, and network organization, highlighting their similarities and differences.

Similarity Assessment

We first evaluated the similarities between the two networks through Pearson correlation analyses at three levels: edge, network, and global. At the edge level, Pearson correlation coefficients were calculated for each connection, comparing the connectivity values derived from GWM-HFN and GM-GM networks. At the network level, we computed the average intra-network and inter-network connectivity strengths across seven functional subnetworks for both methods and analyzed their correlation. Finally, at the global level, the mean connectivity values across all edges were calculated for each participant, and the correlation coefficients across participants were determined to assess the overall consistency between the two approaches.

Variability Assessment

To further compare the two networks, we analyzed their variability across the population by calculating the CV for each edge, defined as the standard deviation divided by the mean. The CV quantifies the relative variability of connection strengths, providing insights into individual differences. This comparison helps reveal whether the GWM-HFN captures unique variability patterns that may reflect its incorporation of white matter pathways. We evaluated the statistical significance of CV differences between the two methods using a bootstrap approach with 10,000 resampling iterations. This step highlights whether the GWM-HFN captures greater or lesser variability compared to the GM-GM network, reflecting its sensitivity to population heterogeneity.

Network Organization Analysis

Lastly, we explored the differences in network organization between the two methods. The Jaccard index was employed to measure the structural similarity between GWM-HFN and GM-GM FC networks for each participant across a range of sparsity thresholds (0.01–0.50, with a step size of 0.01). Additionally, we computed global and local graph-theoretical metrics, including multiple global and local indices, using the DPABINet toolbox[63]. Network comparisons were primarily based on paired t-tests performed on the AUC derived from the 0.10-0.34 sparsity range. These metrics provided a detailed comparison of the topological features of the two networks, revealing unique organizational properties attributable to the inclusion of white matter pathways in the GWM-HFN.

4.7. Age-Related Patterns of GWN-FHN (SALD Dataset)

To investigate age-related patterns and understand how the GWM-HFN evolves over time, we employed linear models to analyze the trajectory of the GWM-HFN throughout adulthood using the SALD dataset. The models considered both linear (in Eq. (1)) and quadratic terms (in Eq. (2)) to capture potential non-linear relationships as shown in the following formula, including sex and head motion (measured by mean FD) as covariables,

$$y = \beta_0^{lin} + \beta_1^{lin} \times Age + \beta_2^{lin} \times Sex + \beta_3^{lin} \times meanFD + \varepsilon, \quad (2)$$

$$y = \beta_0^{qua} + \beta_1^{qua} \times Age + \beta_2^{qua} \times Age^2 + \beta_3^{qua} \times Sex + \beta_4^{qua} \times meanFD + \varepsilon, \quad (3)$$

in which dependent variable is GWM-HFN connectivity strength. The model selection was based on the best description of the trajectory of these measures throughout adulthood, determined by the Akaike Information Criterion (AIC). The significance tests of β_1^{lin} or β_2^{qua} were conducted by t-tests. In the results section, we reported standardized coefficients of β_1^{lin} or β_2^{qua} for the best-fit model. Additionally, for models exhibiting a significant quadratic effect of age, the peak age was calculated using the formula for the axis of symmetry in a quadratic function:

$$Age_{peak} = -\frac{\beta_1^{qua}}{2\beta_2^{qua}}. \quad (4)$$

4.8. Clinical Correlates of GWM-HFN (ABIDE-II Datasets)

To evaluate the clinical relevance of the GWM-HFN framework, we utilized the ABIDE-II dataset, comparing individuals with ASD against TC. Given the multi-site nature of ABIDE-II, we first applied a harmonization procedure to mitigate potential site-related biases. Specifically, the ComBat algorithm[31], implemented via the neuroCombat R package (https://github.com/Jfortin1/neuroCombat_Rpackage/), was used to harmonize the raw GM-WM FC values across acquisition sites before constructing the final GWM-HFN matrices for each participant.

Subsequent group comparisons between ASD and TC participants were conducted on the harmonized GWM-HFN data. First, we compared the global mean connectivity strength between the two groups using a two-sample t-test, including age, sex, and mean FD as covariates. Second, edge-wise group differences were assessed using two-sample t-tests for each connection within the GWM-HFN, again accounting for age, sex, and mean FD. Significance levels for edge-wise comparisons were determined after applying FDR correction for multiple comparisons across all edges. The anatomical distribution of significantly altered connections was summarized by quantifying their membership within seven established functional subnetworks. To benchmark the sensitivity of GWM-HFN against conventional methods, the identical analysis pipeline—including global mean comparison, edge-wise t-tests with covariate control and FDR correction, and network distribution summary—was repeated using traditional GM-GM functional connectivity networks derived from the same participants.

Finally, we investigated the relationship between GWM-HFN connectivity alterations and clinical symptom severity in the ASD group. Specifically, we calculated the Spearman rank correlation between the mean connectivity strength of the GWM-HFN edges showing significant group differences and the participants' total scores on the ADOS_G_TOTAL.

4.9. Behavioral and Cognitive Correlates of GWM-HFN (BGSP Dataset)

The BGSP dataset included a broad range of behavioral and cognitive measures, which allowed examining phenotypic correlates of GWM-HFN. Specifically, we used the PLS regression to examine the ability of GWM-HFN to explain interindividual variance in 4 behavioral and cognitive phenotypes, including shipley vocabulary score, matrix reasoning scores, shipley and matrix reasoning estimated IQ. In the PLS regression model, the response variable was behavioral and cognitive data for a certain domain and the predictor variables were all edges in GM-WM-GM networks. Only the first component of the PLS model (i.e., PLS1) was examined, which was the linear combination of GWM-HFN connections that exhibited the strongest correlation with the behavioral and cognitive data. Significance levels of the correlations were estimated by randomly shuffling the behavioral and cognitive data among participants (10000 times). For each significant correlation, the contribution of a given edge was defined as its weight to form the PLS1.

For measures that showed significant associations with GWM-HFN, we further employed the BBS modeling method[32] to evaluate the predictive capacity of GWM-HFN for individual scores. First, principal component analysis was used for dimensionality reduction by retaining components that explained 80% variance in interregional morphological similarity. Then, a linear regression model was fitted between the expression scores of the retained components and behavioral and cognitive data, which was further used to predict behavioral and cognitive outcomes for unseen participants. Finally, the Pearson correlation between actual scores and predicted values was calculated for each behavioral and cognitive domain. To assess the performance of the BBS model, a ten-fold cross-validation procedure was used. Since a single cross-validation might be sensitive to a particular split of the data into folds[68], the ten-fold cross-validation procedure was repeated 100 times and the resulting mean Pearson

correlation coefficient was reported for each behavioral and cognitive domain. To test whether the Pearson correlation coefficients were significantly higher than random operations, a nonparametric permutation testing procedure was performed by reshuffling the behavioral and cognitive data and repeating the ten-fold cross-validation procedure (10000 times). For each significant correlation, the contribution of a given edge was calculated as the mean value of the product of the coefficient in principal component analysis with the beta value in the linear regression model across all folds and repetitions.

Ethical Statement

All procedures performed in studies involving human participants were in accordance with the ethical standards of the institutional and/or national research committee and with the 1964 Helsinki declaration and its later amendments or comparable ethical standards. This article does not contain any studies with animals performed by any of the authors. Informed consent was obtained from all individual participants included in the study.

Authors Contribution

Ze-Qiang LinLi conceived and designed the overall study. Ze-Qiang LinLi oversaw data collection and verified the analytical methods. Ze-Qiang LinLi, Zhuo-Yan Cai and Kang Hu performed data preprocessing, constructed the networks, and carried out the statistical analyses. Ze-Qiang LinLi, Zhuo-Yan Cai and Kang Hu contributed to the methodology design and drafted large parts of the manuscript. Ze-Qiang LinLi and Chu-Chu Zheng provided critical revisions, shaped the discussion of results, and coordinated manuscript editing. All authors discussed the results, commented on the manuscript at all stages, and approved the final version for publication.

Conflict of Interest Statement

The authors declare that they have no conflict of interest.

Financial support

Ze-Qiang LinLi is supported by the Humanities and Social Sciences Youth Foundation of Ministry of Education of China (24YJCZH164), Guangdong Province General University Characteristic Innovation projects (2024KTSCX178).

Data and Code Availability

Publicly available datasets were analyzed in this study. The analysis code will be made public after the article is accepted.

Reference

1. Biswal, B., Zerrin Yetkin, F., Haughton, V. M. & Hyde, J. S. Functional connectivity in the motor cortex of resting human brain using echo-planar mri. *Magn. Reson. Med.* **34**, 537–541 (1995).
2. Fox, M. D. & Raichle, M. E. Spontaneous fluctuations in brain activity observed with functional magnetic resonance imaging. *Nat. Rev. Neurosci.* **8**, 700–711 (2007).
3. Xia, M., Sun, X., Bu, X., Li, Q. & He, Y. Big connectome imaging data in psychiatric disorders. *Med. Plus* **1**, 100038 (2024).
4. Canario, E., Chen, D. & Biswal, B. A review of resting-state fMRI and its use to examine psychiatric disorders. *Psychoradiology* **1**, 42–53 (2021).
5. Sala-Llonch, R., Bartrés-Faz, D. & Junqué, C. Reorganization of brain networks in aging: A review of functional connectivity studies. *Front Psychol* **6**, 663 (2015).
6. van den Heuvel, M. P. & Hulshoff Pol, H. E. Exploring the brain network: a review on resting-state fMRI functional connectivity. *Eur. neuropsychopharmacol. : j. Eur. Coll. Neuropsychopharmacol.* **20**, 519–34 (2010).
7. Gawryluk, J. R., Mazerolle, E. L. & D'Arcy, R. C. N. Does functional MRI detect activation in white matter? A review of emerging evidence, issues, and future directions. *Front. Neurosci.* **8**, 239 (2014).
8. Grajauskas, L. A., Frizzell, T., Song, X. & D'Arcy, R. C. N. White matter fMRI activation cannot Be treated as a nuisance regressor: overcoming a historical blind spot. *Front. Neurosci.* **13**, 1024 (2019).
9. Chen, G. *et al.* BOLD response is more than just magnitude: improving detection sensitivity through capturing hemodynamic profiles. *Neuroimage* **277**, 120224 (2023).
10. Ji, G.-J. *et al.* Imaging brain white matter function using resting-state functional MRI. *Sci. Bull.* S2095927324007941 (2024) doi:10.1016/j.scib.2024.11.001.
11. Gore, J. C. *et al.* Functional MRI and resting state connectivity in white matter - a mini-review. *Magn. Reson. Imaging* **63**, 1–11 (2019).
12. Peer, M., Nitzan, M., Bick, A. S., Levin, N. & Arzy, S. Evidence for Functional Networks within the Human Brain's White Matter. *J Neurosci* **37**, 6394–6407 (2017).
13. Ding, Z. *et al.* Detection of synchronous brain activity in white matter tracts at rest and under functional loading. *PNAS* **115**, 595–600 (2018).
14. Schilling, K. G. *et al.* Whole-brain, gray, and white matter time-locked functional signal changes with simple tasks and model-free analysis. *PNAS* **120**, 2219666120 (2023).
15. Sengupta, A., Mishra, A., Wang, F., Chen, L. M. & Gore, J. C. Characteristic BOLD signals are detectable in white matter of the spinal cord at rest and after a stimulus. *PNAS* **121**, 2316117121 (2024).
16. Jiang, Y. *et al.* Characteristics of disrupted topological organization in white matter functional connectome in schizophrenia. *Psychol. Med.* **52**, 1333–1343 (2020).
17. Fan, C. *et al.* Altered white matter functional network in nicotine addiction. *Psychiat. Res.* **321**, 115073 (2023).
18. Li, Y. *et al.* Altered white matter functional pathways in alzheimer's disease. *Cerebral Cortex* **34**, (2024).
19. Zhang, Y. *et al.* Desynchronized functional activities between brain white and gray matter in

major depression disorder. *J. magn. reson. imaging : JMRI* **53**, 1375–1386 (2021).
20. LinLi, Z., Hu, K., Guo, Q. & Guo, S. Static and dynamic connectivity structure of white-matter functional networks across the adult lifespan. *Prog. Neuro-Psychopharmacol. Biol. Psychiatry* **136**, 111252 (2025).
21. Borgatti, S. P. & Everett, M. G. Network analysis of 2-mode data. *Soc. Networks* **19**, 243–269 (1997).
22. Gao, Y. *et al.* Functional alterations in bipartite network of white and grey matters during aging. *Neuroimage* **278**, 120277 (2023).
23. Zu, Z. *et al.* The missing third dimension-functional correlations of BOLD signals incorporating white matter. *Sci. Adv.* **10**, 616 (2024).
24. Wang, L. *et al.* fMRI signals in white matter rewire gray matter community organization. *Neuroimage* **297**, 120763 (2024).
25. Xu, L. *et al.* Reductions in the white–gray functional connectome in preclinical alzheimer's disease and their associations with amyloid and cognition. *Alzheimer's Dement.* **20**, 8317–8330 (2024).
26. Noble, S., Scheinost, D. & Constable, R. T. A decade of test-retest reliability of functional connectivity: A systematic review and meta-analysis. *Neuroimage* **203**, 116157 (2019).
27. Pannunzi, M. *et al.* Resting-state fMRI correlations: from link-wise unreliability to whole brain stability. *Neuroimage* **157**, 250–262 (2017).
28. Ilioska, I. *et al.* Connectome-wide mega-analysis reveals robust patterns of atypical functional connectivity in autism. *Biol. Psychiatry* **94**, 29–39 (2023).
29. Koshiyama, D. *et al.* White matter microstructural alterations across four major psychiatric disorders: mega-analysis study in 2937 individuals. *Mol. Psychiatry* **25**, 883–895 (2020).
30. Sato, W. & Uono, S. The atypical social brain network in autism: advances in structural and functional MRI studies. *Curr. Opin. Neurol.* **32**, 617 (2019).
31. Johnson, W. E., Li, C. & Rabinovic, A. Adjusting batch effects in microarray expression data using empirical bayes methods. *Biostatistics* **8**, 118–127 (2007).
32. Sripada, C. *et al.* Basic units of inter-individual variation in resting state connectomes. *Sci. Rep.* **9**, 1900 (2019).
33. Landis, J. R. & Koch, G. G. The measurement of observer agreement for categorical data. *Biometrics* **33**, 159 (1977).
34. Wang, P. *et al.* White Matter Functional Connectivity in Resting-State fMRI: Robustness, Reliability, and Relationships to Gray Matter. *Cereb Cortex* **32**, 1547–1559 (2022).
35. Jain, P., Michael, A. M., Wang, P., Di, X. & Biswal, B. WhiFuN: a toolbox to map the white matter functional networks of the human brain. *Imaging Neuroscience* (2025) doi:10.1162/IMAG.a.3.
36. Honey, C. J. *et al.* Predicting human resting-state functional connectivity from structural connectivity. *Proc. Natl. Acad. Sci.* **106**, 2035–2040 (2009).
37. Sporns, O. & Betzel, R. F. Modular brain networks. *Annu. Rev. Psychol.* **67**, 613–640 (2016).
38. Suárez, L. E., Markello, R. D., Betzel, R. F. & Misic, B. Linking structure and function in macroscale brain networks. *Trends Cognit. Sci.* **24**, 302–315 (2020).
39. Ji, G.-J. *et al.* White matter dysfunction in psychiatric disorders is associated with neurotransmitter and genetic profiles. *Nat. Ment. Health* **1**, 655–666 (2023).
40. Li, J. *et al.* Transcriptomic and macroscopic architectures of intersubject functional variability

in human brain white-matter. *Commun. Biol.* **4**, 1417 (2021).
41. Zhao, B. *et al.* Common genetic variation influencing human white matter microstructure. *Science* **372**, eabf3736 (2021).
42. Dubois, J. & Adolphs, R. Building a science of individual differences from fMRI. *Trends Cognit. Sci.* **20**, 425–443 (2016).
43. Bennett, I. J. & Madden, D. J. Disconnected aging: cerebral white matter integrity and age-related differences in cognition. *Neuroscience* **276**, 187–205 (2014).
44. Madden, D. J., Bennett, I. J. & Song, A. W. Cerebral white matter integrity and cognitive aging: contributions from diffusion tensor imaging. *Neuropsychol. Rev.* **19**, 415–435 (2009).
45. Yeatman, J. D., Wandell, B. A. & Mezer, A. A. Lifespan maturation and degeneration of human brain white matter. *Nat. Commun.* **5**, 4932 (2014).
46. Grady, C. The cognitive neuroscience of ageing. *Nat. Rev. Neurosci.* **13**, 491–505 (2012).
47. Reuter-Lorenz, P. A. & Park, D. C. How does it STAC up? Revisiting the scaffolding theory of aging and cognition. *Neuropsychol. Rev.* **24**, 355–370 (2014).
48. Cabeza, R., Anderson, N. D., Locantore, J. K. & McIntosh, A. R. Aging gracefully: compensatory brain activity in high-performing older adults. *Neuroimage* **17**, 1394–1402 (2002).
49. Travers, B. G. *et al.* Diffusion tensor imaging in autism spectrum disorder: a review. *Autism Res.: Off. J. Int. Soc. Autism Res.* **5**, 289–313 (2012).
50. Wolff, J. J. *et al.* Differences in white matter fiber tract development present from 6 to 24 months in infants with autism. *Am. J. Psychiatry* **169**, 589–600 (2012).
51. Kim, G. S. *et al.* Mapping along-tract white matter microstructural differences in autism. 2025.03.21.644498 Preprint at https://doi.org/10.1101/2025.03.21.644498 (2025).
52. Weber, C. F. *et al.* Age-dependent white matter microstructural disintegrity in autism spectrum disorder. *Front. Neurosci.* **16**, 957018 (2022).
53. Segal, A. *et al.* Multiscale heterogeneity of white matter morphometry in psychiatric disorders. *Biol. Psychiatry: Cognit. Neurosci. Neuroimaging* (2025) doi:10.1016/j.bpsc.2025.03.014.
54. Li, S.-J. *et al.* Alterations of white matter connectivity in preschool children with autism spectrum disorder. *Radiology* **288**, 209–217 (2018).
55. Langen, M., Durston, S., Kas, M. J. H., Van Engeland, H. & Staal, W. G. The neurobiology of repetitive behavior: …and men. *Neurosci. Biobehav. Rev.* **35**, 356–365 (2011).
56. Prat, C. S., Stocco, A., Neuhaus, E. & Kleinhans, N. M. Basal ganglia impairments in autism spectrum disorder are related to abnormal signal gating to prefrontal cortex. *Neuropsychologia* **91**, 268–281 (2016).
57. Binder, J. R., Desai, R. H., Graves, W. W. & Conant, L. L. Where is the semantic system? A critical review and meta-analysis of 120 functional neuroimaging studies. *Cereb. Cortex* **19**, 2767–2796 (2009).
58. Laird, A. R. *et al.* Investigating the functional heterogeneity of the default mode network using coordinate-based meta-analytic modeling. *J. Neurosci.* **29**, 14496–14505 (2009).
59. Seghier, M. L. The angular gyrus. *Neuroscientist* (2012) doi:10.1177/1073858412440596.
60. Haber, S. N. Corticostriatal circuitry. *Dialogues Clin. Neurosci.* (2016) doi:10.31887/DCNS.2016.18.1/shaber.
61. Uddin, L. Q., Supekar, K. S., Ryali, S. & Menon, V. Dynamic reconfiguration of structural and functional connectivity across core neurocognitive brain networks with development. *J*

Neurosci **31**, 18578–89 (2011).
62. Wang, D. *et al.* Parcellating cortical functional networks in individuals. *Nat. Neurosci.* **18**, 1853–1860 (2015).
63. Yan, C.-G., Wang, X.-D., Lu, B., Deng, Z.-Y. & Gao, Q.-L. DPABINet: a toolbox for brain network and graph theoretical analyses. *Sci. Bull.* **69**, 1628–1631 (2024).
64. Rubinov, M. & Sporns, O. Complex network measures of brain connectivity: uses and interpretations. *Neuroimage* **52**, 1059–69 (2010).
65. Watts, D. J. & Strogatz, S. H. Collective dynamics of 'small-world'networks. *Nature* **393**, 440–442 (1998).
66. Girvan, M. & Newman, M. E. J. Community structure in social and biological networks. *Proc. Natl. Acad. Sci.* **99**, 7821–7826 (2002).
67. Eguíluz, V. M., Chialvo, D. R., Cecchi, G. A., Baliki, M. & Apkarian, A. V. Scale-free brain functional networks. *Phys. Rev. Lett.* **94**, 18102 (2005).
68. Varoquaux, G. *et al.* Assessing and tuning brain decoders: cross-validation, caveats, and guidelines. *Neuroimage* **145**, 166–179 (2017).